JCTC Journal of Chemical Theory and Computation

pubs.acs.org/JCTC Article

Benchmark Data Set of Crystalline Organic Semiconductors

Andriy Zhugayevych,* Wenbo Sun, Tammo van der Heide, Carlos R. Lien-Medrano, Thomas Frauenheim, and Sergei Tretiak*

Cite This: J. Chem. Theory Comput. 2023, 19, 8481−8490

ABSTRACT: This work reports a Benchmark Data set of Crystalline Organic Semiconductors to test calculations of the structural and electronic properties of these materials in the solid state. The data set contains 67 crystals consisting of mostly rigid molecules with a single dominant conformer, covering the majority of known structural types. The experimental crystal structure is available for the entire data set, whereas zero-temperature unit cell volume can be reliably estimated for a subset of 28 crystals. Using this subset, we benchmark r^{2}SCAN-D3 and PBE-D3 density functionals. Then, for the entire data set, we benchmark approximate density functional theory (DFT) methods, including GFN1-xTB and DFTB3(3ob-3-1), with various dispersion corrections against r^{2}SCAN-D3. Our results show that r^{2}SCAN-D3 geometries are accurate within a few percent, which is comparable to the statistical uncertainty of experimental data at a fixed temperature, but the unit cell volume is systematically underestimated by 2% on average. The several times faster PBE-D3 provides an unbiased estimate of the volume for all systems except for molecules with highly polar bonds, for which the volume is substantially overestimated in correlation with the underestimation of atomic charges. Considered approximate DFT methods are orders of magnitude faster and provide qualitatively correct but overcompressed crystal structures unless the dispersion corrections are fitted by unit cell volume.

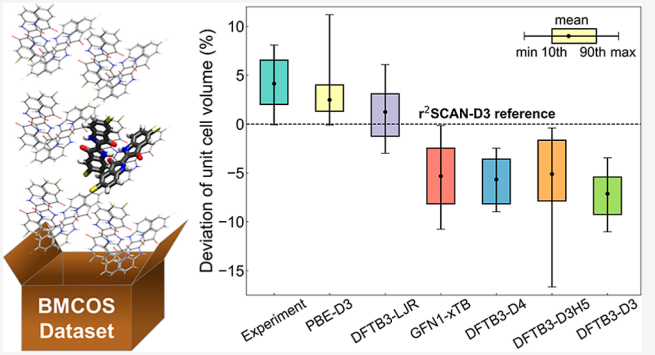

1. INTRODUCTION

The unique optoelectronic properties of organic semiconductors arise from their delocalized π-conjugated electronic system. The task of rational design for these materials for particular applications is a formidable one due to the intricate electronic processes involved and complex structural motifs. In principle, the multiscale structural diversity of organic semiconductors[1] offers great potential for fine-tuning their electronic properties. Nevertheless, achieving accurate and reliable results at a reasonable computational cost necessitates tailored modeling approaches that account for the complexity of their electronic structure and conformational motifs.[2,3] Even for a crystalline morphology, there are uncertainties with atomic positions and polymorph energy ranking because of the omnipresence of various types of disorder and external factors influencing intermolecular packing.[4,5] As a result, significant uncertainties emerge in computed properties, such as charge carrier mobility, as errors accumulate from multiple sources, including molecular geometry and force constant inaccuracies, electronic and vibronic couplings, and the accuracy of the electron−phonon Hamiltonian and its solution methods. Hence, the availability of a benchmark data set for organic semiconductors in their solid-state form is important for assessing the predictive capabilities of computational methods concerning the structural and electronic properties of these materials. This work is aimed to provide such a data set for single crystals, which not only incorporate the most appropriate structural morphology for this purpose but are also of practical use in optoelectronics.[5−8] It should be noted that although a crystal structure can usually be determined experimentally, often materials modeling can be performed only for simulated structures. This includes, for example, crystalline π-conjugated polymers[9] whose atomistic structure can be determined only by a combination of computational and various experimental approaches, including, e.g., vibrational spectroscopy.[10−12]

Over time, numerous large[13−16] and small[17] data sets of crystalline organic semiconductors have been accumulated. However, these data sets were not specifically designed for benchmarking purposes. On the other hand, available benchmark data sets for molecular crystals[18−22] and clusters[23,24] do not contain sufficient samples of extended π-conjugated molecules commonly used in optoelectronic applications.

Received: August 5, 2023
Revised: November 2, 2023
Accepted: November 3, 2023
Published: November 16, 2023

https://doi.org/10.1021/acs.jctc.3c00861
J. Chem. Theory Comput. 2023, 19, 8481−8490

Alternatively, crystals for benchmarking can be taken directly from the Cambridge Structural Database (CSD) or similar heterogeneous sources.[25] However, practitioners should be aware of possible ambiguity in the preprocessing of the raw structural information before benchmarking.

This work introduces the BMCOS1 data set (Benchmark Data set of Crystalline Organic Semiconductors part 1, https://cmsos.github.io/bmcos/) containing 67 crystals, whose molecular structures are explicitly listed in Figures S1 and S2 and Table S8. The index 1 reflects the selection rules for crystals included in the data set: the BMCOS1 is aimed to cover all major classes of single-conformer molecules studied experimentally for potential use in optoelectronics, which have a well-characterized dominating disorder-free crystalline polymorph. Here, a "single-conformer" means that only a single dominant molecular conformation is observed at ambient conditions in solution or the solid state, thus eliminating intramolecular degrees of freedom in the identification of crystal packing. In this sense, flexible dihedrals are acceptable only if the equilibrium geometry is near-planar and rotations have a high energy penalty, e.g., oligothiophenes. Furthermore, for the convenience of benchmarking, the chemical space is limited to the first three rows of the Periodic Table, and the size of the unit cell is capped by about 100 atoms. Moreover, to make the data set suitable for any further analysis of electronic properties, e.g., mapping the wave function of the crystal to molecular orbitals of a symmetric molecule in vacuum, all crystal structures are kept in a unified form: atoms are unfolded to the unit cell, molecules are connected and have the same numbering across the data set, and symmetry-inequivalent molecules are classified by space group orbits.

The selection of chemical moieties to be included in the data set reflects motifs observed in organic semiconductors. Pure hydrocarbons in BMCOS1 are represented mainly by polycyclic aromatic hydrocarbons, including acenes. Sulfur atoms in organic semiconductors occur mainly in the thiophene ring; therefore, BMCOS1 has enough coverage of thienoacenes and oligothiophenes. Tetrathiafulvalene is another sulfur-based π-conjugated moiety included in the data set. Nitrogen is represented by azaacenes, imides, and cyanocarbons. Oxygen is observed mainly in quinone-like structures, though the furan ring and bridging oxygen are also included. Halogens are commonly used in organic semiconductors to tune their properties by hydrogen substitutions, and such molecules are added to BMCOS1 as well. Other nonheavy elements are rare in organic electronics; therefore, we include one molecule per such element: phosphorus in triphenylphosphine, silicon in spirobidibenzosilole, and boron in BODIPY. Branching molecules are usually large in size so we include only their core moieties, such as triphenylene, triphenylbenzene, triptycene, triphenylphosphine, and spirobifluorene, despite these crystals having more than 100 atoms in the unit cell. The largest system included in BMCOS1 is fullerene C60: its 240 atoms in the unit cell substantially exceed the median size of the data set, but it is one of the most commonly used organic semiconductors and represents an important structural motif. On the other side, several small molecules that form semiconductors only as part of larger molecules are added to BMCOS1, in part to make a connection to existing small-molecule data sets, high-level calculations, and extensive experimental studies. The resulting size of the BMCOS1 is consistent with similar data sets for efficient benchmarking by a wide range of methods.

We use density functional theory (DFT) at the r^{2}SCAN-D3 level as the main reference method for BMCOS1. This model incorporates the popular DFT-D3 empirical dispersion correction.[26] The more advanced r^{2}SCAN-D4 should potentially be even more accurate for molecular crystals.[27] However, not all software packages have D4 dispersion corrections implemented, whereas, for the majority of organic molecules, D3 and D4 models demonstrate comparable performance.[28] The commonly used PBE-D3 density functional is much faster than r^{2}SCAN-D3; therefore, it is considered a second reference method. PBE-D3 is particularly important for crystals with hundreds of atoms in the unit cell[29] and for the calculation of force constants, as it might be the top choice DFT-D framework combining reasonable accuracy with practical utility. Hybrid functionals such as CAM-B3LYP-D3 usually provide superior accuracy for both intra- and intermolecular geometries of π-conjugated systems.[9,30] However, these techniques are computationally prohibitive under periodic boundary conditions. Finally because the typical accuracy of both PBE-D3 and r^{2}SCAN-D3 is often higher than the accuracy of extrapolation of available experimental data to zero temperature, the latter cannot serve as a reliable reference geometry for the majority of systems from BMCOS1.

In practice, a single-crystal, disorder-free morphology is rarely observed in organic semiconducting materials, so large supercells are typically needed to obtain a realistic model of a material. Approaching those scales requires computationally efficient and scalable schemes. In this work, we therefore benchmark two classes of approximate DFT methods augmented with dispersion corrections: the Density Functional Tight Binding (DFTB)[31,32] and Geometry, Frequency, Noncovalent, eXtended Tight Binding (GFN-xTB)[33,34] approaches. Among the various DFTB approaches available, we select the DFTB3 method[35] with the PBE-based 3ob-3-1 parametrization[36] covering most elements contained in BMCOS1. Multiple studies have shown that the DFTB3 with dispersion corrections provides a relatively accurate description of organic molecular crystals.[37−39] For the xTB approach, we choose the GFN1-xTB Hamiltonian,[34] providing a relatively accurate description of molecular systems.[33] The GFN2-xTB[40] has been under investigation as well, but we find that many systems from BMCOS1 either relax to unphysical geometries or experience convergence issues arising from the aforementioned fact, preventing us from discussing this method in detail.

The text is organized as follows: we start with a description of the computational methodology used and discuss molecular systems constituting the BMCOS1 data set. We then compare DFT-D results for a subset of BMCOS1 with extensive experimental data and benchmark approximate DFT methods against DFT-D for the entire BMCOS1 data set. Finally, we summarize our observations and conclude.

2. METHODOLOGY

2.1. Reference Computational Methods. All DFT-D calculations of crystals are performed with projector augmented wave (PAW) pseudopotentials as implemented in the VASP program[41] with a 900 eV energy cutoff. For a smaller cutoff, "pulay stress" errors in volume and elastic tensor may become significant. Nevertheless, exploring a reasonable decrease in the cutoff might be helpful for large systems.

https://doi.org/10.1021/acs.jctc.3c00861
J. Chem. Theory Comput. 2023, 19, 8481−8490

Therefore, we have performed calculations with a 600 eV cutoff, where the equilibrium unit cell volume is obtained by fitting the Murnaghan equation of state, whereas all other degrees of freedom are relaxed at a fixed volume. We use a fixed (per crystal) Γ-centered *k*-grid with 0.2 $Å^{-1}$ spacing and 0.2 eV Gaussian smearing. The final energy is calculated with a finer *k*-grid with 0.1 $Å^{-1}$ spacing and the tetrahedron method with Bloch corrections. In all calculations, we use PREC = accurate setting. For the purpose of benchmarking, we have overtightened the convergence criterion for forces to 1 meV/Å, which necessarily requires hundreds of geometry relaxation steps for molecules from the BMCOS1 set. To reach the desired accuracy in forces, the electronic energy tolerance has been set to 0.1−1 μeV (the lower value guarantees accurate forces in cross-checking single-point r^2SCAN-D3 calculations). Furthermore, the Gaussian smearing parameter has been reduced to 0.05 eV for narrow-gap systems such as hexacene. Normally, VASP-default accuracy for electronic energy of 0.1 meV and a slightly decreased threshold for change in total energy during relaxation to 0.1 meV give optimal geometry as accurate as the method itself within less than 100 iterations. The final forces on atoms then typically converge to an order of tens of meV/Å. The primitive cell is used with a predefined basis of primitive vectors unless such an autogenerated shape is too elongated (e.g., chrysene crystal), in which case the lattice reduction is performed. Bulk and shear moduli are derived from the elasticity tensor, according to ref 42.

DFT calculations of molecules in a vacuum are performed using the Gaussian 16 program.[43] As the reference method for single-molecule properties, we use the CAM-B3LYP/Def2-TZVP model chemistry that previously demonstrated robust performance for organic semiconductors.[30]

2.2. Approximate DFT Methods. DFTB and xTB calculations for molecules and crystals are performed using the DFTB+ software package.[44] The first Brillouin zone is sampled by a Γ-centered *k*-grid of at least 0.2 $Å^{-1}$ spacing. Self-consistent charge cycles are performed until the total energy converges to 0.1 μHa (3 μeV). Geometry relaxation is stopped when the maximum absolute gradient component becomes smaller than 0.1 mHa/Bohr (5 meV/Å). We explore four types of dispersion corrections added to DFTB3. Namely, the D3,[45] D4,[28] and DFTB3-D3H5[46] methods as implemented in the DFTB+ package. Additionally, we explore the Lennard-Jones (LJ) potential[47] parametrized as follows: the initial set of LJ parameters (element-wise distances and energies) is taken from the Universal Force Field[48] (UFF), listed in Table S1. Then, the LJ distances and energies are rescaled by 0.9608 and 0.7970 to match the r^2SCAN-D3 equilibrium unit cell volume and binding energy, respectively, for the BMCOS1 data set (Table S2 and Figures S11 and S12). Consequently, we distinguish four DFTB methods: DFTB3-D3, DFTB3-D4, DFTB3-D3H5, and DFTB3-LJR (rescaled UFF). Their parametrization is detailed in Section S3. Following ref,[35] all third-order DFTB3 calculations, except for DFTB3-D3H5, employ a damped γ-function (exponent 4.0) of the Coulomb repulsion between density fluctuations for all interactions involving hydrogen. In the case of DFTB3-D3H5, the hydrogen−hydrogen repulsion per ref 46 has been activated. For GFN1-xTB, we use the standard parametrization described in ref 34.

2.3. Geometry Processing. Initial geometries are taken from the CSD database, except for dibenzoindigo. In the case of multiple CSD entries, we select geometry measured at a lower temperature and by a higher-level method. Original crystallographic information files are processed by the same algorithm and reduced to a canonical form (as described in the BMCOS project webpage). In particular, molecules have the same numbering across the data set to reduce their superposition to simple alignment[49] instead of atom matching.[50] Molecules and crystal geometries are saved in the XYZ file format. In the latter case, the entire Bravais unit cell is stored, translation vectors are denoted by "Tv," and the complete symmetry information is given in the comment line.

2.4. Benchmarking Details. For method comparison, we use multiple parameters: the complete list of definitions is given in Section S1, whereas parameters explicitly discussed in the text are also defined here. The first quantity to compare is the unit cell volume per atom 'V1'; its relative deviation "dV1" is defined as $V1/V1_{ref} - 1$, where "ref" labels a reference method. Deviation in the unit cell shape "dSh" is defined as $\| T/\sqrt[3]{\det T} - T_{ref}/\sqrt[3]{\det T_{ref}} \|$, where T is the matrix of translation vectors, the norm is Frobenius, and the matrices are superimposed to minimize the norm. Translations and rotations of individual molecules relative to a reference are denoted as displacement "dr" and deflection angle "phi." The difference in the intramolecular geometry is denoted as "dev" and is calculated as the root-mean-square deviation of atom positions excluding hydrogens. Here, both molecules are superimposed to minimize this deviation. Finally, the binding energy per molecule "Eb" is calculated with respect to a fully relaxed molecule in vacuum (planar conformation is taken for nonrigid molecules). Relative and dimensionless deviations are given in percents. For all scalar and vector quantities, we calculate the "method error" over the data set using several scalar parameters ("vectors are treated as sequences of independent scalars): mean value ("mean," "ave"), root-mean square value, 90th percentile ("90th"), and maximum value ("max"). The BMCOS project webpage (https://cmsos.github.io/bmcos/) contains the BMCOS1 data set files and other relevant information.

3. STRUCTURAL TYPES IN BMCOS1 DATA SET

The BMCOS1 data set is aimed to cover all structural types of potentially high-performing organic semiconductors consisting of relatively small molecules (tens of atoms) without nonconjugated side chains. First and foremost, the herringbone packing of acenes and heteroacenes, such as pentacene and DNTT (dinaphthothienothiophene), enables superior two-dimensional charge carrier mobility.[7] There are several subtypes of this motif[25] covered in the data set, including one interdigitated structure IF12b (6,12-dihydroindeno[1,2-*b*]fluorene), which potentially might increase the dimensionality of the electronic connectivity network.

The columnar packing of slipped π-stacks is another commonly observed crystalline motif for conjugated molecules.[51] This structure fosters a large and robust intermolecular electronic coupling network along the stacks, whereas the interstack couplings are typically small. This class in the BMCOS1 data set is represented by several systems with different levels of interdigitation between stacks, ranging from coronene to NDI (naphthalenetetracarboxdiimide).

Hydrogen-deficient (H-poor) molecules bring forward another type of intermolecular contacts in terms of electronic couplings. Here, the limiting cases are fullerenes and TCNQ-F4 (tetrafluoro-tetracyanoquinodimethane), which have no

https://doi.org/10.1021/acs.jctc.3c00861
J. Chem. Theory Comput. 2023, 19, 8481−8490

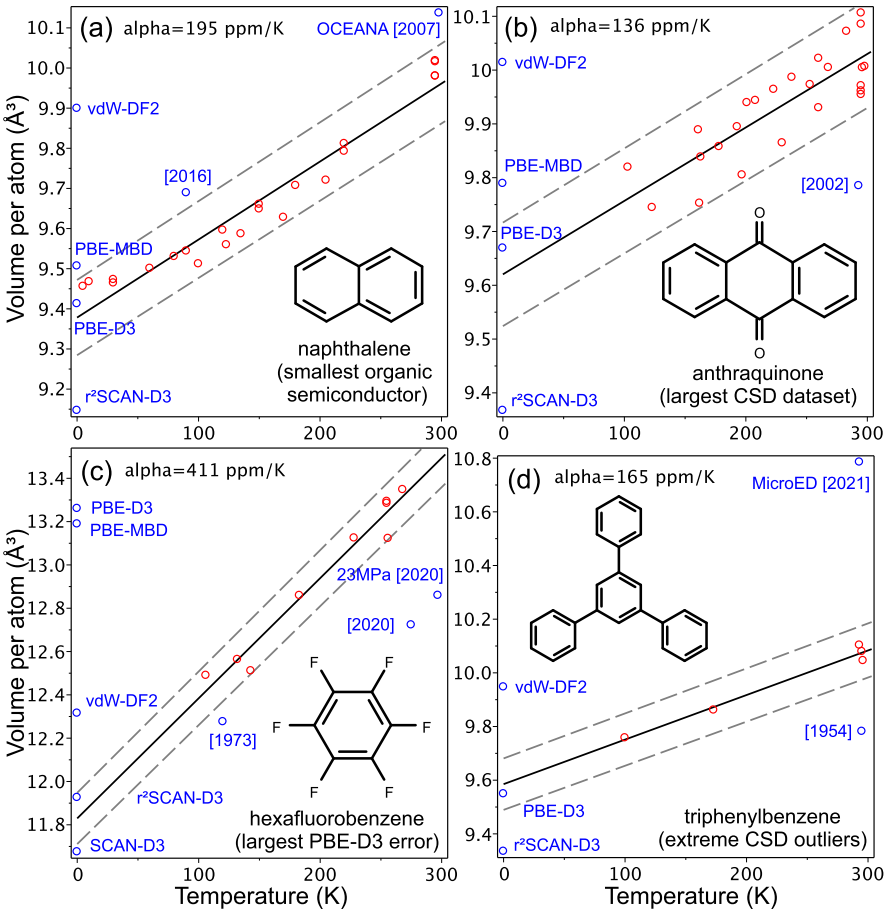

Figure 1. Thermal expansion of the selected molecular crystals. Dashed lines mark a 1% deviation. Red dots show experimental data from the CSD database used for linear fit. Blue dots are outliers (publication year is given) and DFT calculations (at 0 K).

hydrogen atoms. Instead, the surface of such molecules is terminated with π-conjugated atoms and functional groups[52] such as halogens, oxygen as in quinones, cyano (CN), and nitro (NO_2) groups. All of these terminations are represented in BMCOS1. Further, aromatic nitrogen and bridging chalcogens (e.g., in thiazolothiazole) stand at the molecular surface, forming unobscured intermolecular contacts between π-conjugated segments. Consequently, regardless of packing, H-poor molecules usually form small but numerous electronic contacts, which are non-negligible. This is especially the case for heavy electron-rich atoms like chalcogens and halogens, allowing for shortened interatomic contacts.[53,54]

Other known structural types are represented by larger molecules involving flexible conjugated backbones and solubilizing side chains, which are beyond the immediate scope of the BMCOS1 data set. This includes two important crystalline motifs: brickwork packing observed for TIPS-pentacene and wire mesh packing appearing for some acceptor−donor−acceptor molecules.[29] Electronic connectivity in these crystals is conducted via a π-stack type of intermolecular contact, so that, partially, these materials are represented in BMCOS1. Further, several short flexible linear oligomers have been added, including oligo(thiophene) and oligo(*p*-phenylenevinylene) motifs. Flexible branching oligomers have conformational complexity, which typically leads to high disorder and low charge carrier mobility. Nevertheless, they are widely used as charge transporting layers (e.g., as host materials) in organic electronics.[55] In principle, there are no fundamental limitations to their performance as semiconductors. Therefore, we have included in our data set some small representatives of this class, such as triphenylbenzene, and only branching core moieties, such as benzotrithiophene.

Across a broad variety of structural motifs observed for molecular crystals, some materials have large electronic couplings but were never recognized as semiconductors,[56] thus motivating exploration of these structural types of organic semiconductors. As such, we have included two more classes of molecules sparsely studied for organic electronics. The first one has rigid (fused) branching or star-shaped molecules, represented by tetrathienophenazine.[57] The other includes nonplanar (nonfullerene) π-conjugated molecules, triptycene, and spirobifluorene.

4. BENCHMARKING OF REFERENCE DFT-D METHODS AGAINST EXPERIMENTAL DATA

DFT-D benchmarking for relaxed optimized geometries requires a reference low-temperature experimental crystal structure corrected for quantum effects, which might be around 1% in volume[58] and even larger for large-amplitude modes.[30] Since it is rarely available for molecular semiconductor crystals, we only test the unit cell volume extrapolated to 0 K from elevated temperatures. Such extrapolation can be reliably performed for 28 crystals from the BMCOS1 data set (these have at least 3 data points in a broad temperature range within 1% deviation from a line,

https://doi.org/10.1021/acs.jctc.3c00861
J. Chem. Theory Comput. 2023, 19, 8481−8490

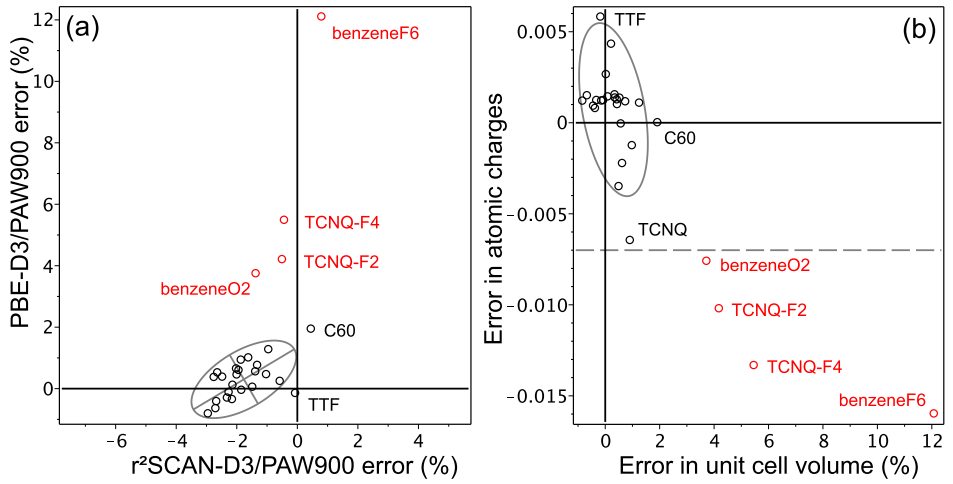

Figure 2. (a) r²SCAN-D3 and PBE-D3 errors for unit cell volume; see Table 1 for explanations. The ellipse is drawn for 2σ with red dots excluded. (b) Correlation plot for PBE-D3 errors for the unit cell volume vs its errors for the Hirshfeld atomic charges relative to CAM-B3LYP functional with TZVP basis.

Table S9). For C60, both rotationally ordered and disordered polymorphs are used in the extrapolation since their thermal coefficients are statistically indistinguishable for the available data. Because the temperature range is relatively small, resulting in only a ~5% volume change at 300 K, we use a linear fit. Thermal expansion data for selected crystals are summarized in Figure 1. Deviations of available experimental data at a fixed temperature are usually smaller than 1%, whereas outliers come from older data and less accurate measurement techniques. Derived thermal expansion coefficients agree well with studies on large data sets.[59] Subsequently, a value of 150 ppm/K can be taken as a rough universal coefficient for the entire BMCOS1 data set. Modeling of thermal expansion and thermodynamic quantities is possible for simple molecular crystals,[60] but it becomes computationally demanding for large unit cells.

Results of benchmarking of r²SCAN-D3 and PBE-D3 for the 28 crystals subset are shown in Figure 2 and Table 1. The

Table 1. Benchmarking DFT-D Against Experiment for the Unit Cell Volume for 28 Crystals From BMCOS1[a]

	r²SCAN-D3	PBE-D3	subset
median	−1.8	0.4	0.4
mean	−1.6	1.2	0.3
standard dev.	1.0	2.6	0.6
lower decile	−2.7	−0.4	−0.5
upper decile	−0.1	4.1	1.1
min	−2.9	−0.8	−0.8
max	0.8	12.1	1.9

[a]Available experimental data in the CSD data set are extrapolated to 0 K. All numbers are deviations in percent. The "subset" column shows PBE-D3 data with four crystals excluded based on PBE errors in atomic charges (red dots in Figure 2b). See details in Table S10

r²SCAN-D3 systematically underestimates the unit cell volume by 1−2% in consistency with the ref 27 conclusion that the r²SCAN-D4 slightly overbinds molecular crystals. Overall, it shows robust performance with a very small range of errors across the entire set of 28 systems. In contrast, PBE-D3 fails to predict the unit cells for two semiconductors, TCNQ-F4 and TCNQ-F2, substantially overestimating their volumes. To check if this error is related to the terminal electronegative atoms, we have added hexafluorobenzene (benzeneF6) and benzoquinone (benzeneO2) to the BMCOS1 data set. Markedly, PBE-D3 fails for these two molecular crystals as well. To be able to predict such failures, we notice that errors in the unit cell volume correlate well with errors in the Hirshfeld atomic charges, Figure 2b. As such, if we exclude molecules with large errors in the atomic charges (dashed line in Figure 2b), the performance of PBE-D3 on the reduced subset becomes superior except for C60; typically, it is accurate within 1% in the volume. Additional study on special data sets (e.g., ref 61) is needed to pinpoint the problem. Evidently, the influence of intermolecular halogen contacts is critical: the PBE-D3 error for trichlorotrifluorobenzene is similar to that for hexafluorobenzene, whereas for trifluorobenzene, it is substantially smaller, and the error in volume for triazine is vanishing. Interestingly, for narrow-gap molecules such as long acenes,[62] PBE-D3 produces accurate intermolecular geometry despite predicting very inaccurate electronic structure (see, e.g., calculated gaps in the BMCOS project webpage).

A comparison of calculated and measured crystal structures for the entire BMCOS1 data set can only be made given the uncertainty of thermal expansion effects, which are usually anisotropic and larger than the accuracy of DFT-D. In such comparisons, we will always set a specific DFT-D method as the reference because experimental data are obtained with different approaches and at different temperatures. For the unit cell volume, we can apply the aforementioned universal thermal expansion coefficient (150 ppm/K) to all crystals with insufficient data. The result is shown in Figure 3 and is consistent with the above study of 28 systems. Furthermore, it shows that overall thermal effects across the entire BMCOS1 data set are about a few percent in volume, that is about 1% on a linear scale. Neglecting these effects leads to a systematic bias clearly visible in the green and red histograms in Figure 3. Among other geometrical parameters, we can compare those that are less sensitive to thermal expansion to avoid any extrapolation to 0 K: the shape of the unit cell, the orientation of molecules, and intramolecular geometry (excluding hydrogens), using one scalar descriptor per each property ("dSh", "phi," and "dev," respectively, as defined in Section S1). For both r²SCAN-D3 and PBE-D3, on average, the shape deviates

https://doi.org/10.1021/acs.jctc.3c00861
J. Chem. Theory Comput. 2023, 19, 8481−8490

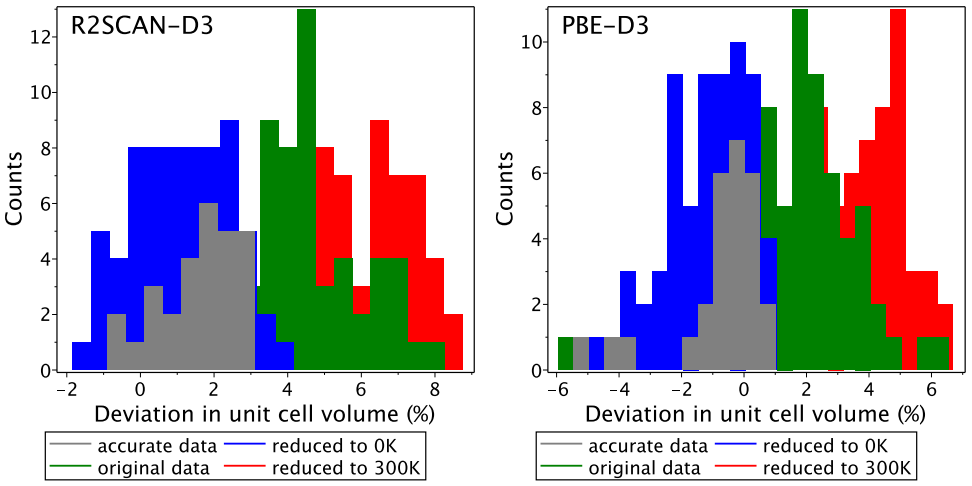

Figure 3. Relative difference between the unit cell volume derived from experimental data and its value relaxed with the r^{2}SCAN-D3 and PBE-D3 methods. Different sets correspond to different treatments of thermal expansion. In "accurate data," we use the extrapolated to 0 K volume available for a subset of 28 crystals. In "original data," thermal expansion is ignored, whereas in "reduced" data, the geometries are extrapolated to a given temperature by the best-estimated thermal expansion coefficients. The latter are either derived from the available experimental data (37 crystals, including the "accurate data" subset) or set to 150 ppm/K. Out of scale are benzene at 300 K and benzeneF6 at 0 K for PBE-D3, and benzene, benzeneF6, benzeneO2, and BODIPY at 300 K for r^{2}SCAN-D3.

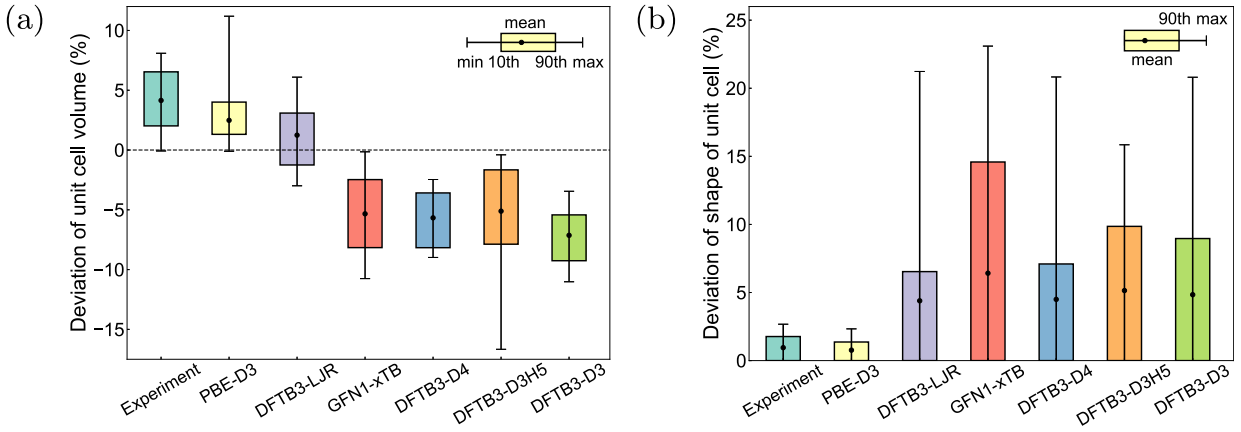

Figure 4. Benchmark of approximate DFT methods against r^{2}SCAN-D3 for (a) unit cell volume and (b) shape. Here, the experimental data are not extrapolated to zero temperature.

by 1%, the orientation deflects by 1°, and the intramolecular geometry differs by tens of mÅ (Tables S11−S12). It should be noted that the large difference in intramolecular geometry for rigid molecules might indicate reduced fidelity of experimental data (e.g., the two outliers, dibenzoindigo and naphthodithiophene (NDT) in Figures S3−S4).

Modeling of molecular crystals has its own specific challenges[60] which can be analyzed using the BMCOS1 data set. First of all, these are soft systems in the sense that many collective structural motions have a complex flat potential energy surface (PES). Moreover, there is no clear separation between these motions and the other nuclear degrees of freedom. Instead, there is a continuous distribution of vibrational frequencies, raising up to typical bond stretching values (without counting phonon dispersion). For our data set, the lowest frequencies at the Γ-point range from 1.5 meV for triptycene to 8 meV for TCNQ-F2 with one molecule per primitive cell (both molecules are rigid and relatively small). Three crystals have imaginary frequencies in PBE-D3 due to the brute-force use of finite differences. Linear PES scans for these modes show that they correspond to complex collective motions with energy changes as small as tenths of meV per unit cell upon mass-weighted displacement of 0.5 Å (Figures S5−S7). Similarly, the lowest eigenvalue of the elastic matrix[63] is often very small. For PBE-D3, there is one crystal with a negative elastic modulus due to the use of finite differences: a relaxed PES scan along two unit cell parameters shows a positive-definite quadratic PES, but the energy changes only by tens of μeV per atom upon 1% deformation (Figure S8 and Table S4).

The BMCOS1 data set represents organic semiconductors with relatively small unit cells, whereas the majority of materials used in organic electronics have more complex structures. Therefore, it is important to have methods that are scalable to hundreds of atoms in the unit cell. This requirement immediately screens out the r^{2}SCAN functional, which is slightly less accurate (though more reliable) and substantially slower than the PBE model (Figure S9). Next, the convergence criteria can be relaxed to a default tolerance for the wave function and 1−2 orders of magnitude tighter convergence for geometry relaxation, yielding geometries with subpercent accuracy (Table S15) and practically converged

https://doi.org/10.1021/acs.jctc.3c00861
J. Chem. Theory Comput. 2023, 19, 8481−8490

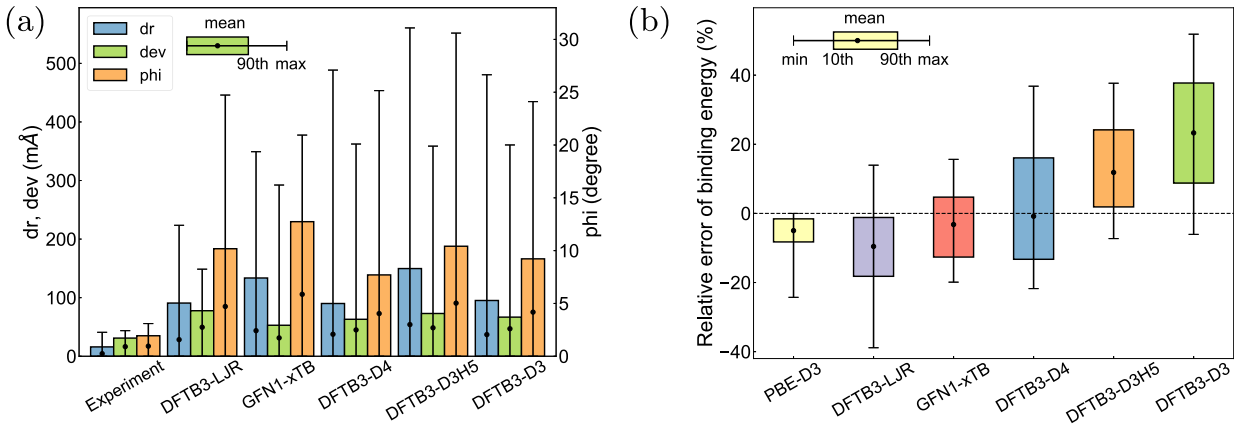

Figure 5. Benchmark of approximate DFT methods against r^{2}SCAN-D3 reference for (a) intramolecular ("dev") and intermolecular (displacement "dr" and deflection "phi") geometries and (b) binding energy.

binding energies. In terms of the wave function, important parameters influencing computational cost are the plane-wave energy cutoff and k-grid spacing. The former is critical for unit cell optimization and elastic matrix calculation. In particular, unconstrained relaxation of the unit cell with a 600 eV cutoff systematically underestimates its volume by about 3%, which is substantially larger than the error of PBE-D3 (Table S16). Coarse k-grids produce meaningful results for organic semiconductors due to their large electronic band gaps and small band dispersions, especially for geometry relaxation: a grid with 0.2 Å^{-1} spacing gives final gradients essentially the same as those produced by finer grids (Table S17). Smaller k-grids are still acceptable within the accuracy of DFT-D itself up to 2 × 2 × 2 grid, corresponding to the spacing of about 0.5 Å^{-1} for small unit cells (Table S18). At the same time, ignoring electronic dispersion in directions where molecules have close contact with their periodic images leads to poor results (Tables S7 and S18). This is valid for most systems except probably for long molecules such as pentacene, where the precise position of the herringbone layers with respect to each other is no longer important.

5. BENCHMARKING OF APPROXIMATE DFT METHODS AGAINST DFT-D

For benchmarking the approximate DFT methods, we take the r^{2}SCAN-D3 results as the reference because this method is more reliable than the PBE-D3 model. Notably, the typical difference between these two DFT-D approaches for calculated geometries (Table S13) is much smaller than the difference between the reference and the approximate DFT methods. In this section, the complete data set has been employed for benchmarking. However, DFTB methods exclude BODIPY and spirobidibenzosilole due to the lack of boron and silicon parameters in the 3ob-3-1 set.

Figure 4 summarizes the accuracy of the optimized crystal geometries. As illustrated in Figure 4a, all methods underestimate the r^{2}SCAN-D3 unit cell volume except for DFTB3-LJR, which was tuned to match the r^{2}SCAN-D3 equilibrium unit cell volume and binding energy, as described in Section 2. In terms of the unit cell shape (Figures 4b and S10), the DFTB3 methods exhibit higher accuracy compared to the GFN1-xTB techniques, especially DFTB3-LJR and DFTB3-D4. Other structural parameters describing the intramolecular geometry and molecular arrangement inside the unit cell are given in Figure 5a. For the intermolecular arrangement ("dr" and "phi"), most DFTB3 methods demonstrate higher accuracy than their GFN1-xTB counterpart, whereas for the intramolecular geometry ("dev"), the trend is opposite.

The performance of approximate DFT methods in terms of the binding energy at relaxed geometries is shown in Figure 5b. Overall, errors in energies and volume correlate (Figure 4a), albeit with a larger magnitude of deviations from DFT-D. The most accurate method is GFN1-xTB; its energies are unbiased with respect to DFT-D but have a larger spread of deviations compared to the PBE-D3 reference. However, the relaxed geometries obtained by the GFN1-xTB method exhibit large deviations in the unit cell volume and shape (Figure 4), so that accurate binding energies may result from some error compensation. Further insights can be gained from Figure S13, where GFN1-xTB binding energies are calculated for the relaxed r^{2}SCAN-D3 geometries, showing a systematic underestimation of the DFT-D reference energies by several percent.

To study the chemical space dependence of the performance of approximate DFT methods, the entire BMCOS1 data set was partitioned into several groups based on their chemical composition (Table S19). The group-specific benchmarks (Figure S14) show that the considered DFTB methods are more accurate for pure hydrocarbons, whereas the largest errors in geometry come from systems with sulfur, chlorine, cyano-group, and combinations of several light chemical elements (CNH(O) group in Table S19). In contrast, GFN1-xTB shows uniform performance (with large error dispersion) across the entire chemical space. In order to further identify the outliers in the DFTB3-LJR and GFN1-xTB methods, a comparative analysis against experimental data is presented in Figure S15. Similar to PBE-D3, systems with polar bonds (TCNQ family and hexafluorobenzene) are among the outliers for both methods, though the trend is less systematic. Other outliers are coronene for DFTB3-LJR and tetrathiafulvalene (TTF) for GFN1-xTB.

6. CONCLUSIONS

The diversity of organic semiconductors has grown tremendously in the last two decades, triggering the concomitant development of various modeling approaches. Except for several thoroughly studied systems, the majority of available experimental and calculated data contain large uncertainties due to the multiscale complexity of these materials. At the same time, no high-level theoretical methods exist to provide robust reference data for bulk organic semiconductors except

https://doi.org/10.1021/acs.jctc.3c00861
J. Chem. Theory Comput. 2023, 19, 8481−8490

for a few molecular crystals with a small enough number of atoms in the unit cell. The proposed BMCOS1 data set serves the purpose of testing modeling methods for the structural and electronic properties of organic semiconductors made up of relatively rigid π-conjugated molecules. Among the computationally feasible DFT-D methods considered, r^{2}SCAN-D3 proves to be the most reliable, while PBE-D3 emerges as the most accurate method for predicting the unit cell volume within 1% accuracy, with the exception of molecules where PBE produces inaccurate atomic charges. When it comes to scalability, PBE-D3 continues to be the primary choice for crystals with hundreds of atoms in the unit cell. However, there is a possibility of overestimating the lengths of intermolecular contacts involving fluorine atoms. To address this issue in a computationally efficient manner, further investigation is required, including an assessment of the potential importance of range separation in dispersion interactions. In this study, all DFTB3- and xTB-based methods utilizing a universal parametrization exhibit reasonable accuracy, albeit with a consistent underestimation of the unit cell volume by several percentage points. However, this bias can be rectified by rescaling the parameters of the dispersion corrections, as demonstrated in the DFTB3-LJR method.

Altogether, the BMCOS1 database lays the foundation for the creation of various benchmark-type data sets for organic semiconductors, to include polymorphs, flexible molecules, polymers, metal−organic systems, and more. Our current data set not only provides a platform for designing and testing reduced atomistic quantum-mechanical models aiming to achieve DFT-D accuracy for molecular solids but also serves as a crucial reference and training set for assessing advanced interatomic potentials, including those generated through machine learning methodologies.[64]

■ ASSOCIATED CONTENT

Supporting Information

The Supporting Information is available free of charge at https://pubs.acs.org/doi/10.1021/acs.jctc.3c00861.

Technical details of calculations and a snapshot of the database (core files) (ZIP)

(PDF)

■ AUTHOR INFORMATION

Corresponding Authors

Andriy Zhugayevych − *Max Planck Institute for Polymer Research, 55128 Mainz, Germany;* orcid.org/0000-0003-4713-1289; Email: andriy.zhugayevych@mpip-mainz.mpg.de

Sergei Tretiak − *Los Alamos National Laboratory, Los Alamos, New Mexico 87545, United States;* orcid.org/0000-0001-5547-3647; Email: serg@lanl.gov

Authors

Wenbo Sun − *Bremen Center for Computational Materials Science, 28359 Bremen, Germany;* orcid.org/0000-0001-6297-6728

Tammo van der Heide − *Bremen Center for Computational Materials Science, 28359 Bremen, Germany;* orcid.org/0000-0002-0304-192X

Carlos R. Lien-Medrano − *Bremen Center for Computational Materials Science, 28359 Bremen, Germany;* orcid.org/0000-0001-7696-8366

Thomas Frauenheim − *Bremen Center for Computational Materials Science, 28359 Bremen, Germany*

Complete contact information is available at: https://pubs.acs.org/10.1021/acs.jctc.3c00861

Funding

Open access funded by Max Planck Society.

Notes

The authors declare no competing financial interest.

■ ACKNOWLEDGMENTS

A.Z. thanks Denis Andrienko for the helpful discussions. T.v.d.H. acknowledges financial support from the German Research Foundation (DFG) through Grant no. FR2833/76-1. S.T. acknowledges the support of the Humboldt Research Award (Germany). The work at Los Alamos National Laboratory (LANL) was supported by the LANL Directed Research and Development Funds (LDRD) and performed in part at the Center for Integrated Nanotechnologies (CINT), a US Department of Energy (DOE) Office of Science user facility at LANL.

■ REFERENCES

(1) Rivnay, J.; Mannsfeld, S. C. B.; Miller, C. E.; Salleo, A.; Toney, M. F. Quantitative Determination of Organic Semiconductor Microstructure from the Molecular to Device Scale. *Chem. Rev.* **2012**, *112*, 5488−5519.

(2) Bhat, V.; Callaway, C.; Risko, C. Computational Approaches for Organic Semiconductors: From Chemical and Physical Understanding to Predicting New Materials. *Chem. Rev.* **2023**, *123*, 7498−7547.

(3) Oberhofer, H.; Reuter, K.; Blumberger, J. Charge Transport in Molecular Materials: An Assessment of Computational Methods. *Chem. Rev.* **2017**, *117*, 10319−10357.

(4) Davey, R. J.; Schroeder, S. L. M.; ter Horst, J. H. . Nucleation of Organic Crystals—A Molecular Perspective. *Angew. Chem., Int. Ed.* **2013**, *52*, 2166−2179.

(5) Zhang, X.; Dong, H.; Hu, W. Organic Semiconductor Single Crystals for Electronics and Photonics. *Adv. Mater.* **2018**, *30*, 1801048.

(6) Jiang, H.; Hu, W. The Emergence of Organic Single Crystal Electronics. *Angew. Chem., Int. Ed.* **2020**, *59*, 1408−1428.

(7) Wang, C.; Dong, H.; Jiang, L.; Hu, W. Organic semiconductor crystals. *Chem. Soc. Rev.* **2018**, *47*, 422−500.

(8) Chen, J.; Zhang, W.; Wang, L.; Yu, G. Recent Research Progress of Organic Small-Molecule Semiconductors with High Electron Mobilities. *Adv. Mater.* **2023**, *35*, 2210772.

(9) Zhugayevych, A.; Mazaleva, O.; Naumov, A.; Tretiak, S. Lowest-energy crystalline polymorphs of P3HT. *J. Phys. Chem. C* **2018**, *122*, 9141−9151.

(10) Harrelson, T. F.; Cheng, Y. Q.; Li, J.; Jacobs, I. E.; Ramirez-Cuesta, A. J.; Faller, R.; Moule, A. J. Identifying Atomic Scale Structure in Undoped/Doped Semicrystalline P3HT Using Inelastic Neutron Scattering. *Macromol* **2017**, *50*, 2424−2435.

(11) Kapaev, R.; Zhugayevych, A.; Ryazantsev, S.; Aksyonov, D.; Novichkov, D.; Matveev, P.; Stevenson, K. Charge storage mechanisms of a pi-d conjugated polymer for advanced alkali-ion battery anodes. *Chem. Sci.* **2022**, *13*, 8161−8170.

(12) Harrelson, T.; Dantanarayana, V.; Xie, X.; Koshnick, C.; Nai, D.; Fair, R.; Nunez, S.; Thomas, A.; Murrey, T.; Hickner, M.; Grey, J.; Anthony, J.; Gomez, E.; Troisi, A.; Faller, R.; Moule, A. Direct probe of the nuclear modes limiting charge mobility in molecular semiconductors. *Mater. Horiz.* **2019**, *6*, 182−191.

(13) Organic Materials Database (OMDB), https://omdb.mathub.io (accessed 04 28, 2023). .

(14) Borysov, S.; Geilhufe, R.; Balatsky, A. Organic materials database: An open-access online database for data mining. *PLoS One* **2017**, *12*, No. e0171501.
(15) Organic Crystals in Electronic and Light-Oriented Technologies (OCELOT) database, https://oscar.as.uky.edu (accessed 04 28, 2023).
(16) Ai, Q.; Bhat, V.; Ryno, S.; Jarolimek, K.; Sornberger, P.; Smith, A.; Haley, M.; Anthony, J.; Risko, C. OCELOT: An infrastructure for data-driven research to discover and design crystalline organic semiconductors. *J. Chem. Phys.* **2021**, *154*, 174705.
(17) Yavuz, I.; Lopez, S. A.; Lin, J. B.; Houk, K. N. Quantitative prediction of morphology and electron transport in crystal and disordered organic semiconductors. *J. Mater. Chem. C* **2016**, *4*, 11238−11243.
(18) Reilly, A. M.; Cooper, R. I.; Adjiman, C. S.; Bhattacharya, S.; Boese, A. D.; Brandenburg, J. G.; Bygrave, P. J.; Bylsma, R.; Campbell, J. E.; Car, R.; et al. Report on the sixth blind test of organic crystal structure prediction methods. *Acta Cryst. B* **2016**, *72*, 439−459.
(19) Brandenburg, J. G.; Grimme, S. Organic crystal polymorphism: a benchmark for dispersion-corrected mean-field electronic structure methods. *Acta Cryst. B* **2016**, *72*, 502−513.
(20) Dolgonos, G.; Hoja, J.; Boese, A. Revised values for the X23 benchmark set of molecular crystals. *Phys. Chem. Chem. Phys.* **2019**, *21*, 24333−24344.
(21) Control and Prediction of the Organic Solid State (CPOSS) database. http://www.chem.ucl.ac.uk/cposs (accessed 04 28, 2023).
(22) Price, S. Control and prediction of the organic solid state: a challenge to theory and experiment <sup/>. *Proc. R. Soc. A* **2018**, *474*, 20180351.
(23) Sure, R.; Grimme, S. Comprehensive Benchmark of Association (Free) Energies of Realistic Host-Guest Complexes. *J. Chem. Theory Comput.* **2015**, *11*, 3785−3801.
(24) Sedlak, R.; Janowski, T.; Pitoňák, M.; Řezáč, J.; Pulay, P.; Hobza, P. Accuracy of Quantum Chemical Methods for Large Noncovalent Complexes. *J. Chem. Theory Comput.* **2013**, *9*, 3364−3374.
(25) Schatschneider, B.; Monaco, S.; Liang, J.; Tkatchenko, A. High-Throughput Investigation of the Geometry and Electronic Structures of Gas-Phase and Crystalline Polycyclic Aromatic Hydrocarbons. *J. Phys. Chem. C* **2014**, *118*, 19964−19974.
(26) Grimme, S.; Antony, J.; Ehrlich, S.; Krieg, H. A consistent and accurate ab initio parametrization of density functional dispersion correction (DFT-D) for the 94 elements H-Pu. *J. Chem. Phys.* **2010**, *132*, 154104.
(27) Ehlert, S.; Huniar, U.; Ning, J.; Furness, J.; Sun, J.; Kaplan, A.; Perdew, J.; Brandenburg, J. r2SCAN-D4: Dispersion corrected meta-generalized gradient approximation for general chemical applications. *J. Chem. Phys.* **2021**, *154*, 061101.
(28) Caldeweyher, E.; Ehlert, S.; Hansen, A.; Neugebauer, H.; Spicher, S.; Bannwarth, C.; Grimme, S. A generally applicable atomic-charge dependent London dispersion correction. *J. Chem. Phys.* **2019**, *150*, 154122.
(29) Halaby, S.; Martynowycz, M. W.; Zhu, Z.; Tretiak, S.; Zhugayevych, A.; Gonen, T.; Seifrid, M. Microcrystal Electron Diffraction for Molecular Design of Functional Non-Fullerene Acceptor Structures. *Chem. Mater.* **2021**, *33*, 966−977.
(30) Tukachev, N. V.; Maslennikov, D. R.; Sosorev, A. Y.; Tretiak, S.; Zhugayevych, A. Ground state geometry and vibrations of polyphenylenevinylene oligomers. *J. Phys. Chem. Lett.* **2019**, *10*, 3232−3239.
(31) Cui, Q.; Elstner, M. Density functional tight binding: values of semi-empirical methods in an ab initio era. *Phys. Chem. Chem. Phys.* **2014**, *16*, 14368−14377.
(32) Elstner, M.; Porezag, D.; Jungnickel, G.; Elsner, J.; Haugk, M.; Frauenheim, T.; Suhai, S.; Seifert, G. Self-consistent-charge density-functional tight-binding method for simulations of complex materials properties. *Phys. Rev. B* **1998**, *58*, 7260−7268.
(33) Bannwarth, C.; Caldeweyher, E.; Ehlert, S.; Hansen, A.; Pracht, P.; Seibert, J.; Spicher, S.; Grimme, S. Extended tight-binding quantum chemistry methods. *Wiley Interdiscip. Rev.: Comput. Mol. Sci.* **2021**, *11*, No. e1493.
(34) Grimme, S.; Bannwarth, C.; Shushkov, P. A Robust and Accurate Tight-Binding Quantum Chemical Method for Structures, Vibrational Frequencies, and Noncovalent Interactions of Large Molecular Systems Parametrized for All spd-Block Elements (Z. = 1−86). *J. Chem. Theory Comput.* **2017**, *13*, 1989−2009.
(35) Gaus, M.; Cui, Q.; Elstner, M. DFTB3: Extension of the Self-Consistent-Charge Density-Functional Tight-Binding Method (SCC-DFTB). *J. Chem. Theory Comput.* **2011**, *7*, 931−948.
(36) Kubillus, M.; Kubař, T.; Gaus, M.; Řezáč, J.; Elstner, M. Parameterization of the DFTB3Method for Br, Ca, Cl, F, I, K, and Na in Organic and Biological Systems. *J. Chem. Theory Comput.* **2015**, *11*, 332−342.
(37) Brandenburg, J.; Grimme, S. Accurate Modeling of Organic Molecular Crystals by Dispersion-Corrected Density Functional Tight Binding (DFTB). *J. Phys. Chem. Lett.* **2014**, *5*, 1785−1789.
(38) Mortazavi, M.; Brandenburg, J.; Maurer, R.; Tkatchenko, A. Structure and Stability of Molecular Crystals with Many-Body Dispersion-Inclusive Density Functional Tight Binding. *J. Phys. Chem. Lett.* **2018**, *9*, 399−405.
(39) Dolgonos, G.; Boese, A. Adjusting dispersion parameters for the density-functional tight-binding description of molecular crystals. *Chem. Phys. Lett.* **2019**, *718*, 7−11.
(40) Bannwarth, C.; Ehlert, S.; Grimme, S. GFN2-xTB - An Accurate and Broadly Parametrized Self-Consistent Tight-Binding Quantum Chemical Method with Multipole Electrostatics and Density-Dependent Dispersion Contributions. *J. Chem. Theory Comput.* **2019**, *15*, 1652−1671.
(41) Kresse, G.; Furthmuller, J. Efficient Iterative Schemes for Ab Initio Total-Energy Calculations Using a Plane-Wave Basis Set. *Phys. Rev. B* **1996**, *54*, 11169−11186.
(42) Sewell, T.; Menikoff, R.; Bedrov, D.; Smith, G. A molecular dynamics simulation study of elastic properties of HMX. *J. Chem. Phys.* **2003**, *119*, 7417−7426.
(43) Frisch, M. J.; *Gaussian 16*, Revision C.01; Gaussian Inc, Wallingford CT, 2016.
(44) Hourahine, B.; Aradi, B.; Blum, V.; Bonafe, F.; Buccheri, A.; Camacho, C.; Cevallos, C.; Deshaye, M.; Dumitrică, T.; Dominguez, A.; Ehlert, S.; Elstner, M.; van der Heide, T.; Hermann, J.; Irle, S.; Kranz, J.; Kohler, C.; Kowalczyk, T.; Kubař, T.; Lee, I.; Lutsker, V.; Maurer, R.; Min, S.; Mitchell, I.; Negre, C.; Niehaus, T.; Niklasson, A.; Page, A.; Pecchia, A.; Penazzi, G.; Persson, M.; Řezáč, J.; Sanchez, C.; Sternberg, M.; Stohr, M.; Stuckenberg, F.; Tkatchenko, A.; Yu, V.; Frauenheim, T. DFTB+, a software package for efficient approximate density functional theory based atomistic simulations. *J. Chem. Phys.* **2020**, *152*, 124101.
(45) Grimme, S.; Ehrlich, S.; Goerigk, L. Effect of the damping function in dispersion corrected density functional theory. *J. Comput. Chem.* **2011**, *32*, 1456−1465.
(46) Řezáč, J.; Hobza, P. Advanced Corrections of Hydrogen Bonding and Dispersion for Semiempirical Quantum Mechanical Methods. *J. Chem. Theory Comput.* **2012**, *8*, 141−151.
(47) Zhechkov, L.; Heine, T.; Patchkovskii, S.; Seifert, G.; Duarte, H. An Efficient a Posteriori Treatment for Dispersion Interaction in Density-Functional-Based Tight Binding. *J. Chem. Theory Comput.* **2005**, *1*, 841−847.
(48) Rappe, A.; Casewit, C.; Colwell, K.; Goddard, W.; Skiff, W. UFF, a full periodic table force field for molecular mechanics and molecular dynamics simulations. *J. Am. Chem. Soc.* **1992**, *114*, 10024−10035.
(49) Kearsley, S. K. On the orthogonal transformation used for structural comparisons. *Acta Cryst. A* **1989**, *45*, 208−210.
(50) Honig, S.; Lemmen, C.; Rarey, M. Small molecule superposition: A comprehensive overview on pose scoring of the latest methods. *Wiley Interdiscip. Rev.: Comput. Mol. Sci.* **2023**, *13*, No. e1640.
(51) Gray, M.; Herbert, J. Origins of Offset-Stacking in Porous Frameworks. *J. Phys. Chem. C* **2023**, *127*, 2675−2686.

(52) Zhugayevych, A.; Postupna, O.; Wang, H. L.; Tretiak, S. Modification of optoelectronic properties of conjugated oligomers due to donor/acceptor functionalization: DFT study. *Chem. Phys.* **2016**, *481*, 133−143.
(53) Landrum, G. A.; Hoffmann, R. Secondary bonding between chalcogens or pnicogens and halogens. *Angew. Chem., Int. Ed.* **1998**, *37*, 1887−1890.
(54) Zhugayevych, A.; Lubchenko, V. Electronic structure and the glass transition in pnictide and chalcogenide semiconductor alloys. I. The formation of the *ppσ*-network. *J. Chem. Phys.* **2010**, *133*, 234503.
(55) Poriel, C.; Rault-Berthelot, J. Designing Host Materials for the Emissive Layer of Single-Layer Phosphorescent Organic Light-Emitting Diodes: Toward Simplified Organic Devices. *Adv. Funct. Mater.* **2021**, *31*, 2010547.
(56) Schober, C.; Reuter, K.; Oberhofer, H. Virtual Screening for High Carrier Mobility in Organic Semiconductors. *J. Phys. Chem. Lett.* **2016**, *7*, 3973−3977.
(57) Xie, Y.; Fujimoto, T.; Dalgleish, S.; Shuku, Y.; Matsushita, M.; Awaga, K. Synthesis, optical properties and charge transport characteristics of a series of novel thiophene-fused phenazine derivatives. *J. Mater. Chem. C* **2013**, *1*, 3467−3481.
(58) Ko, H.; DiStasio, R.; Santra, B.; Car, R. Thermal expansion in dispersion-bound molecular crystals. *Phys. Rev. Mater.* **2018**, *2*, 055603.
(59) van der Lee, A.; Dumitrescu, D. Thermal expansion properties of organic crystals: a CSD study. *Chem. Sci.* **2021**, *12*, 8537−8547.
(60) Hoja, J.; Reilly, A. M.; Tkatchenko, A. First-principles modeling of molecular crystals: structures and stabilities, temperature and pressure. *Wiley Interdiscip. Rev.: Comput. Mol. Sci.* **2016**, *7*, No. e1294.
(61) Thalladi, V.; Weiss, H.; Blaser, D.; Boese, R.; Nangia, A.; Desiraju, G. R. C−H···F Interactions in the Crystal Structures of Some Fluorobenzenes. *J. Am. Chem. Soc.* **1998**, *120*, 8702−8710.
(62) Dupuy, N.; Casula, M. Fate of the open-shell singlet ground state in the experimentally accessible acenes: A quantum Monte Carlo study. *J. Chem. Phys.* **2018**, *148*, 134112.
(63) Mouhat, F.; Coudert, F. Necessary and sufficient elastic stability conditions in various crystal systems. *Phys. Rev. B* **2014**, *90*, 224104.
(64) Anstine, D.; Isayev, O. Machine Learning Interatomic Potentials and Long-Range Physics. *J. Phys. Chem. A* **2023**, *127*, 2417−2431.

https://doi.org/10.1021/acs.jctc.3c00861
J. Chem. Theory Comput. 2023, 19, 8481−8490

Supporting Information for
Benchmark dataset of crystalline organic semiconductors

Andriy Zhugayevych,*† Wenbo Sun,‡ Tammo van der Heide,‡ Carlos R. Lien-Medrano,‡ Thomas Frauenheim,‡ Sergei Tretiak*¶

†*Max Planck Institute for Polymer Research, Ackermannweg 10, 55128 Mainz, Germany*
‡*Bremen Center for Computational Materials Science, Am Fallturm 1, 28359 Bremen, Germany*
¶*Los Alamos National Laboratory, NM 87545, United States*

*E-mail: andriy.zhugayevych@mpip-mainz.mpg.de; serg@lanl.gov

November 2, 2023

S1 Computational methodology: abbreviations and notations

a3p	Ahlrichs triple-ζ basis Def2-TZVP	MD	Molecular Dynamics
AO	Atomic Orbital	MO	Molecular Orbital
BMCOS	Benchmark Dataset of Crystalline Organic Semiconductors	MWD	Mass-Weighted Displacement
		PAW	Projector Augmented Wave
CIF	Crystallographic Information File	PES	Potential Energy Surface
CSD	Cambridge Structural Database	p2p	Pople double-ζ polarized basis 6-31G*
EoS	Equation of State	RMS	Root-Mean Square
DFT	Density Functional Theory	SCF	Self-Consistent Field
DFT-D	Dispersion-corrected DFT	TB	Tight Binding
DFTB	Density Functional based Tight Binding	ZPE	Zero-Point Energy
HOMO	Highest Occupied Molecular Orbital		
LUMO	Lowest Unoccupied Molecular Orbital		

BMCOS dataname notations (alphabetical order) [URL]

To minimize use of special symbols we denote Ao=Å, deg=degree (angle), iX=X^(-1), X/mol=X per molecule, dX=deviation of X in % except for angles.

- `[a,b,c,alpha,beta,gamma]` (Ao,deg) unit cell parameters
- `[dr,phi,dev]` (mAo,deg,mAo) displacement, deflection, and RMS deviation of single-molecule geometry without hydrogens (molecules are superimposed individually by MolMod/Superimpose, the result is RMS-averaged over all symmetry-unique molecules)
- `al=alpha` (ppm/K) thermal expansion coefficient
- `conf` conformation or configuration
- `dbet` (deg) absolute deviation of monoclinic angle
- `dHOMO,dLUMO` (eV) energy gap between HOMO/LUMO and next HOMO/LUMO
- `dlen` (%) deviation of length of translation vectors (three-dimensional vector)
- `dSh` (%) deviation of shape of unit cell, the same as `dTv` but with volume rescaled to unity
- `dTv` (%) RMS deviation of translation vectors (Frobenius norm of the unit cell matrix divided by square root of the number of translation vectors) divided by cubic root of the unit cell volume (the compared unit cell is rotated to minimize this RMS deviation, the code is BasicTools/SuperimposeM)
- `Eb` (eV/mol) binding energy
- `el` list of chemical elements
- `EM,EM1` (GPa) elastic matrix (elasticity tensor in Voigt notation) and its lowest eigenvalue
- `freq1` (meV) lowest vibrational frequency
- `gap` (eV) HOMO-LUMO gap
- `id=sys` BMCOS system identifier, usually a common name of a molecule
- `K,GR,GV` (GPa) bulk and shear moduli calculated from `EM` by MolMod/exam_vas/PrintFreq [Sewell03]
- `K0,K0'` (GPa,1) bulk modulus and its derivative calculated by Murnaghan equation of state fit, the code is MolMod/EOSfit
- `mult=m` number of primitive cells in Bravais unit cell
- `na` number of atoms in unit cell
- `na1,nas,nu=Z` number of atoms in the smallest repeating unit, list of number of atoms in molecules from this unit, and number of such units
- `name` IUPAC-consistent chemical name of a molecule
- `nb` number of electronic bands (NBANDS)
- `nd` number of data points
- `ng` number of elements in `SG`
- `nkp` number of k-points
- `nm` number of molecules in unit cell (usually Bravais unit cell)
- `no` number of symmetry-unique molecules, i.e. number of orbits in `orbs`
- `nopt` number of geometry relaxation iterations
- `nscf` number of SCF iterations
- `nstab=ns` number of elements in point symmetry group (stabilizer) of molecules in crystal
- `orbs` symmetry-generated orbits of molecules in unit cell as list of lists of molecule indexes
- `PG` point group
- `pubchem` PubChem identifier
- `SG` symmetry group or space group if combined with `PG`
- `T` (K) temperature
- `td` (days) wall-clock computing time in days
- `Up2=|G|,maxG` (meV/Ao) RMS norm and maximum absolute force on atoms
- `V` (Ao^3) unit cell volume
- `V0` (Ao^3) volume per atom extrapolated to 0K
- `V1` (Ao^3) volume per atom

S2 List of molecules

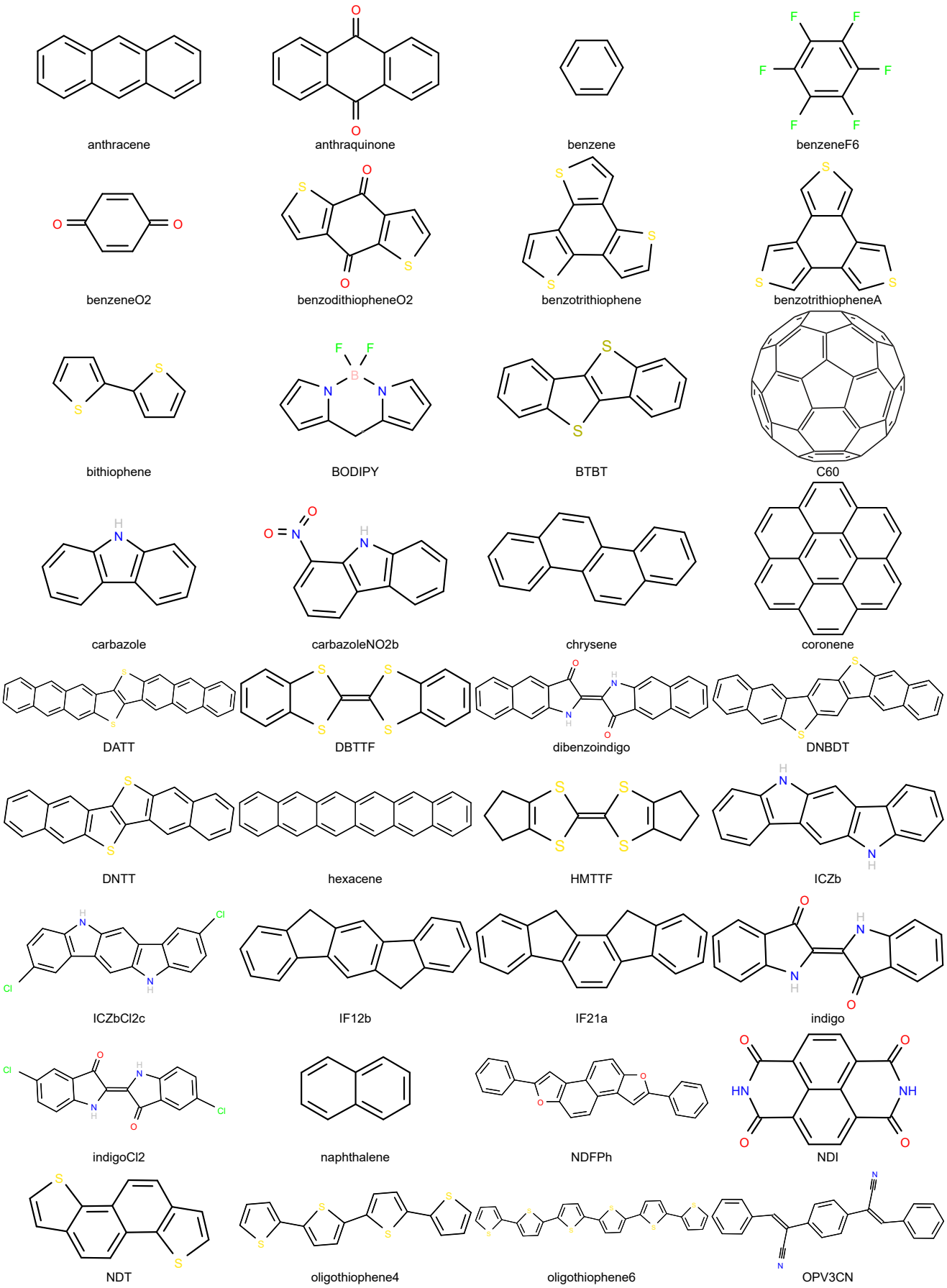

Figure S1: List of molecules, part 1: A-O.

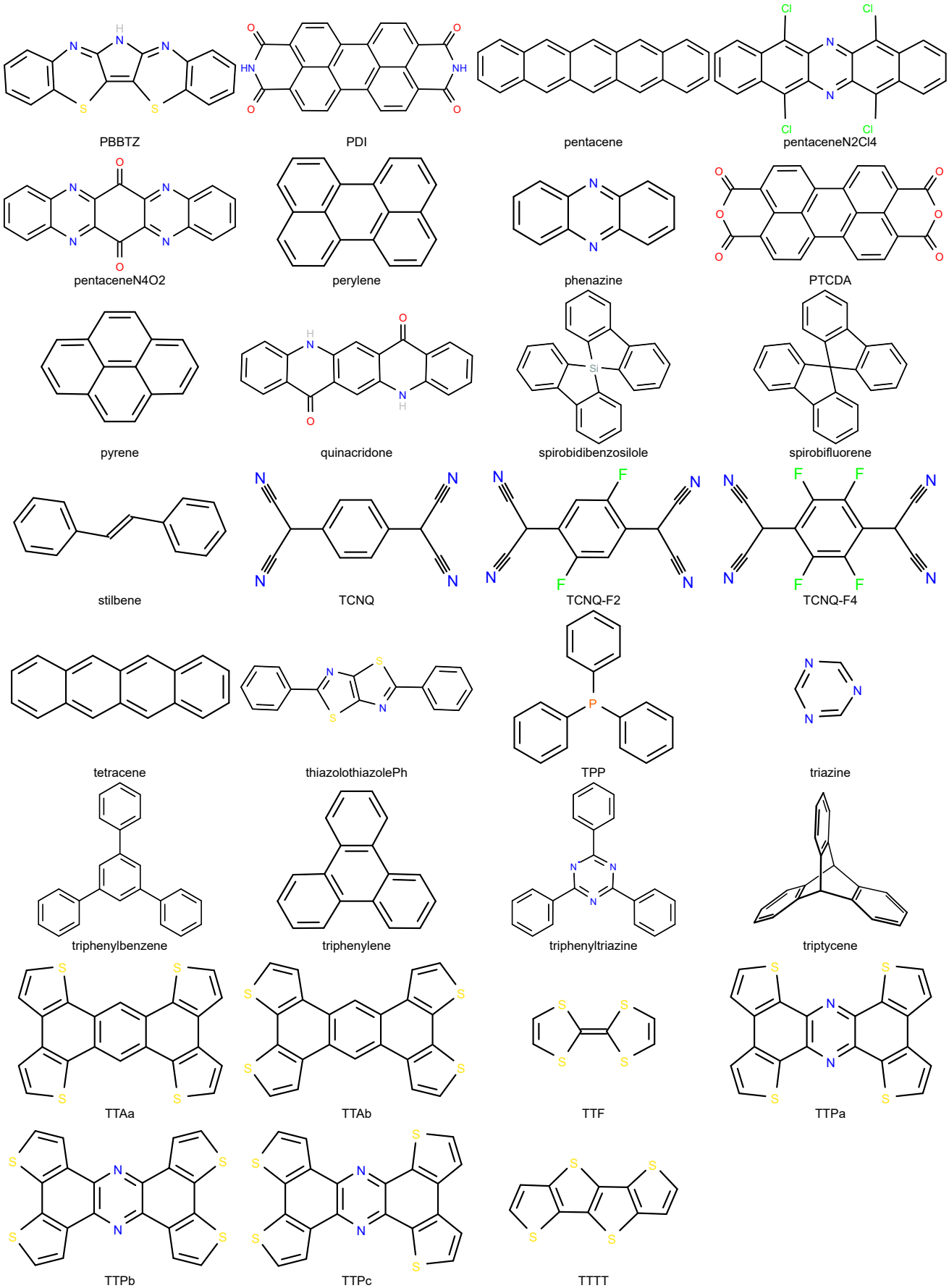

Figure S2: List of molecules, part 2: P-Z.

S3 DFTB parameters

Table S1: Lennard–Jones dispersion parameters used in DFTB3-LJ method.

elements	distance x_{I}^{a} [Å]	D_{I}^{c} [kcal/mol]
H	2.886	0.044
C	3.851	0.105
N	3.660	0.069
O	3.500	0.060
F	3.364	0.050
P	4.147	0.305
S	4.035	0.274
Cl	3.947	0.227

Table S2: Lennard–Jones dispersion parameters used in the DFTB3-LJR method. The UFF distances and energies of Table S1 have been rescaled by 0.9608 and 0.7970 respectively, according to the average signed deviation of Fig. S11 and Fig. S12.

elements	distance x_{I}^{a} [Å]	D_{I}^{c} [kcal/mol]
H	2.7728688	0.035068
C	3.7000408	0.083685
N	3.5165280	0.054993
O	3.3628000	0.047820
F	3.2321312	0.039850
P	3.9844376	0.243085
S	3.8768280	0.218378
Cl	3.7922776	0.180919

Table S3: Becke–Johnson damping parameters used in the DFTB3-D3(BJ) method.

parameters	s_6	s_8	a_1	a_2 [a_0]
3ob-3-1	1.0	3.209	0.746	4.191

Table S4: Zero-damping parameters used in the DFTB3-D3H5 method.

parameters	s_6	s_8	$s_{r,6}$	α_6
3ob-3-1	1.0	0.49	1.25	29.61

Table S5: H5 hydrogen correction parameters used in the DFTB3-D3H5 method.

parameters	s_r	s_w	k_{OH}	k_{NH}	k_{SH}
3ob-3-1	0.714	0.25	0.06	0.18	0.21

Table S6: Becke–Johnson damping parameters used in the DFTB3-D4(BJ) method.

parameters	s_6	s_8	s_9	a_1	a_2 [a_0]
3ob-3-1	1.0	0.6635015	1.0	0.5523240	4.3537076

S4 Supporting model systems

Table S7: Dependence of the electronic band energy of a half-filled dimerized chain on boundary conditions (TB model of trans-polyacetylene and its annulenes). Here t and t' are transfer integrals of primary ("double") and secondary ("single") bonds. In this model the monomer is a pair of sites connected by the primary bond. These monomers are interconnected by weak secondary bonds. We divide the total energy by number of monomers and subtract the electronic energy of the monomer, $-2t$, so that the result is the band contribution to the binding energy of monomers in a chain. Here E' is the complementary complete elliptic integral. Notice that in terms of electronic levels, circle of N monomers is equivalent to the infinite chain on a finite Γ-centered grid with N k-points. In this context, Γ-point calculations introduce an "extra-bond" artifact, $2t'$. In 2 k-points calculations the secondary bonding energy is missing, which is acceptable for molecular crystals without strong donor-acceptor intermolecular interactions.

Boundary conditions	Binding energy	Expanded in t'/t
infinite chain	$\frac{4}{\pi}(t+t')\mathrm{E}'\left(\frac{t-t'}{t+t'}\right)-2t$	$\frac{t'^2}{2t}+\frac{t'^4}{32t^3}$
circle of 4 monomers	$\sqrt{t^2+t'^2}-t$	$\frac{t'^2}{2t}-\frac{t'^4}{8t^3}$
circle of 3 monomers	$\frac{4}{3}\sqrt{t^2-tt'+t'^2}-\frac{4}{3}t+\frac{2}{3}t'$	$\frac{t'^2}{2t}+\frac{t'^3}{4t^2}+\frac{t'^4}{32t^3}$
circle of 2 monomers	0	0
circle of 1 monomer	$2t'$	$2t'$
dimer	$\sqrt{4t^2+t'^2}-2t$	$\frac{t'^2}{4t}-\frac{t'^4}{64t^3}$

S5 Additional figures and tables copied from the project webpage

Table S8: Datasheets: core data [URL].

sys	conf	na1	nm	na	el	SG1	SG	pubchem	name
benzene	cryst	12	4	48		6/mmm	Pbca	241	benzene
naphthalene	cryst	18	2	36		mmm	P21/c	931	naphthalene
anthracene	cryst	24	2	48		mmm	P21/c	8418	anthracene
tetracene	cryst	30	2	60		mmm	P-1	7080	tetracene
pentacene	cryst	36	2	72		mmm	P-1	8671	pentacene
hexacene	cryst	42	2	84		mmm	P-1	123044	hexacene
chrysene	cryst	30	4	120		2/m	C2/c	9171	chrysene
pyrene	cryst	26	4	104		mmm	P21/c	31423	pyrene
perylene	cryst	32	2	64		mmm	P21/c	9142	perylene
IF12b	cryst	34	2	68		2/m	P21/c	15559295	6,12-dihydroindeno[1,2-b]fluorene
IF21a	cryst	34	4	136		mm2	P21/c	15559296	11,12-dihydroindeno[2,1-a]fluorene
triphenylene	cryst	30	4	120		-62m	P212121	9170	triphenylene
coronene	cryst	36	2	72		6/mmm	P21/c	9115	coronene
stilbene	cryst	26	4	104		2/m	P21/c	638088	stilbene
triazine	cryst	9	4	36	N	-62m	C2/c	9262	s-triazine
phenazine	cryst	22	2	44	N	mmm	P21/c	4757	phenazine
carbazole	cryst	22	4	88	N	mm2	Pnma	6854	carbazole
ICZb	cryst	32	2	64	N	2/m	P21/c	114764	indolo[3,2-b]carbazole
TCNQ	cryst	20	4	80	N	mmm	C2/c	73697	tetracyanoquinodimethane
TCNQ-F2	cryst	20	2	40	NF	2/m	C2/m	5255840	2,5-difluoro-7,7,8,8-tetracyanoquinodimethane
TCNQ-F4	cryst	20	4	80	NF	mmm	Pbca	2733307	2,3,5,6-tetrafluoro-7,7,8,8-tetracyanoquinodimethane
ICZbCl2c	cryst	32	2	64	NCl	2/m	P21/c	66722443	2,8-dichloroindolo[3,2-b]carbazole
pentaceneN2Cl4	cryst	34	2	68	NCl	mmm	P21/c	91402528	5,7,12,14-tetrachloro-6,13-diazapentacene
TTTT	cryst	18	2	36	S	2/m	P21/c	14383681	thieno[3,2-b]thieno[2',3':4,5]thieno[2,3-d]thiophene
BTBT	cryst	24	2	48	S	2/m	P21/c	136056	[1]Benzothieno[3,2-b][1]benzothiophene
DNTT	cryst	36	2	72	S	2/m	P21	51050187	dinaphtho[2,3-b:2',3'-f]thieno[3,2-b]thiophene
DATT	cryst	48	2	96	S	2/m	P21	53308489	dianthra[2,3-b:2',3'-f]thieno[3,2-b]thiophene
DNBDT	cryst	42	2	84	S	2/m	P21/c	57913385	dinaphtho[2,3-d:2',3'-d']benzo[1,2-b:4,5-b']dithiophene
NDT	cryst	24	4	96	S	2/m	P21/c	58434773	naphtho[1,2-b:5,6-b']dithiophene
bithiophene	cryst	16	2	32	S	2/m	P21/c	68120	bithiophene
oligothiophene4	cryst	30	2	60	S	2/m	P21/c	86618470	quaterthiophene
oligothiophene6	cryst	44	2	88	S	2/m	P21/c	11340899	sexithiophene
benzotrithiophene	cryst	21	4	84	S	-6	P21/c	44225674	benzo[1,2-b:3,4-b':5,6-b'']trithiophene
benzotrithiopheneA	cryst	21	4	84	S	-62m	P21	2762442	benzo[1,2-c:3,4-c':5,6-c'']trithiophene
TTF	cryst	14	2	28	S	mmm	P21/c	99451	tetrathiafulvalene
HMTTF	cryst	28	4	112	S	mmm	P21/c	625027	hexamethylene-tetrathiafulvalene
DBTTF	cryst	26	2	52	S	mmm	P21/c	141136	dibenzotetrathiafulvalene
benzeneF6	cryst	12	6	72	F	6/mmm	P21/c	9805	hexafluorobenzene
benzeneO2	cryst	12	2	24	O	mmm	P21/c	4650	benzoquinone
anthraquinone	cryst	24	2	48	O	mmm	P21/c	6780	anthraquinone
PTCDA	cryst	38	2	76	O	mmm	P21/c	67191	perylenetetracarboxylic dianhydride
NDFPh	cryst	44	2	88	O	2/m	P21/c	89963552	naphtho[2,1-b:6,5-b']difuran
NDI	cryst	26	2	52	NO	mmm	P-1	79771	naphthalene-1,8:4,5-tetracarboxydiimide
PDI	cryst	40	2	80	NO	mmm	P21/c	66475	perylenediimide
quinacridone	cryst	36	2	72	NO	2/m	P21/c	13976	quinacridone
pentaceneN4O2	cryst	32	2	64	NO	mmm	P21/c	101507809	quinoxalino[2,3-b]phenazine-6,13-dione
indigo	cryst	30	2	60	NO	2/m	P21/c	10215	indigo
indigoCl2	cryst	30	2	60	NOCl	2/m	P21/c	136653217	5,5'-dichloroindigo
dibenzoindigo	cryst	42	2	84	NO	2/m	P21/c	0	dibenzoindigo
carbazoleNO2b	cryst	24	4	96	NO	m	P21/c	96730	1-nitrocarbazole
TTAa	cryst	36	2	72	S	mmm	P21/c	90727247	1,2:4,3:5,6:8,7-tetra(epithioetheno)anthracene
TTAb	cryst	36	2	72	S	mmm	P21/c	101860588	3,4,10,11-tetrathiatetracyclopenta[a,c,h,j]anthracene
TTPa	cryst	34	2	68	NS	mmm	P21/c	101566660	1,2:4,3:5,6:8,7-tetra(epithioetheno)phenazine
TTPb	cryst	34	4	136	NS	mmm	P21/c	102314304	3,4,10,11-tetrathiatetracyclopenta[a,c,h,j]phenazine
TTPc	cryst	34	2	68	NS	mm2	P21	0	m-tetrathienophenazine
PBBTZ	cryst	30	4	120	NS	mm2	P21/c	91574055	6h-pyrrolo[3,2-b:4,5-b']bis[1,4]benzothiazine
thiazolothiazolePh	cryst	30	2	60	NS	2/m	P21/c	240920	2,5-diphenyl(1,3)thiazolo(5,4-d)(1,3)thiazole
benzodithiopheneO2	cryst	18	2	36	OS	2/m	P21/c	288478	benzo[1,2-b:4,5-b']dithiophene-4,8-dione
C60	cryst	60	4	240		m-5	Pa-3	123591	buckminsterfullerene
triptycene	cryst	34	4	136		-62m	P212121	92764	triptycene
BODIPY	cryst	21	8	168	NFB	mm2	C2/c	25058173	4,4-difluoro-4-bora-3a,4a-diaza-s-indacene
OPV3CN	cryst	42	4	168	N	2/m	Pbca	54520030	1,4-bis(1-cyano-2-phenylethenyl)benzene
spirobifluorene	cryst	41	4	164		-42m	P21/c	135975	9,9'-spirobi[9H-fluorene]
spirobidibenzosilole	cryst	41	4	164	Si	-42m	P41212	135976	5,5'-spirobi(dibenzosilole)
triphenyltriazine	cryst	39	4	156	N	-62m	P21/c	10305	triphenyl-1,3,5-triazine
triphenylbenzene	cryst	42	4	168		32	Pna21	11930	1,3,5-triphenylbenzene
TPP	cryst	34	4	136	P	3	P21/c	11776	triphenylphosphine

Table S9: Datasheets: experimental data [URL].

sys	conf	T	al	nd	Tmin	Tmax	V1vsT
benzene	cryst	100	353	11	15	270	V0=9.51(7)
naphthalene	cryst	100	195	22	5	295	V0=9.378(19)
anthracene	cryst	94	179	22	90	295	V0=9.336(13)
tetracene	cryst	175	142	4	175	295	V0=9.31(11)
pentacene	cryst	180	183	16	90	498	V0=9.10(5)
hexacene	cryst	123	123	3	123	295	alpha(300K)=123
chrysene	cryst	125	184	3	125	295	V0=9.262(7)
pyrene	cryst	93	172	11	90	295	V0=9.610(16)
perylene	cryst	200	104	3	130	295	V0=9.192(2)
IF12b	cryst	296					OJONIL
IF21a	cryst	100					OJICOA
triphenylene	cryst	123	116	6	123	295	V0=9.33(4)
coronene	cryst	100	139	11	100	296	V0=9.534(16)
stilbene	cryst	90	194	20	90	373	V0=9.36(2)
triazine	cryst	5	138	2	5	150	alpha(300K)=138
phenazine	cryst	295	173	6	80	296	V0=9.65(4)
carbazole	cryst	100	179	6	100	295	V0=9.16(2)
ICZb	cryst	293					VARMUY
TCNQ	cryst	180	117	10	100	295	V0=12.31(3)
TCNQ-F2	cryst	180	184	5	100	295	V0=12.32(8)
TCNQ-F4	cryst	180	198	5	100	295	V0=13.181(19)
ICZbCl2c	cryst	113					VARNAF
pentaceneN2Cl4	cryst	150					UTEFEF
TTTT	cryst	295					JOTVAP
BTBT	cryst	100	89	5	90	293	V0=10.91(2)
DNTT	cryst	293					NICLAN
DATT	cryst	293					AVIBEN
DNBDT	cryst	298					MOGQAC
NDT	cryst	293					OKUPEQ
bithiophene	cryst	133	235	2	133	173	alpha(300K)=235
oligothiophene4	cryst	295	154	4	150	295	alpha(300K)=154
oligothiophene6	cryst	295					ZAQZUM
benzotrithiophene	cryst	293					ERIKIZ
benzotrithiopheneA	cryst	120					KISFEY
TTF	cryst	290	208	5	98	295	V0=13.53(4)
HMTTF	cryst	296					KIVDAV
DBTTF	cryst	123	148	3	123	295	V0=11.66(3)
benzeneF6	cryst	106	411	9	106	268	V0=11.83(9)
benzeneO2	cryst	173	313	4	113	298	V0=10.31(10)
anthraquinone	cryst	163	136	25	103	298	V0=9.62(4)
PTCDA	cryst	223					SUWMIG
NDFPh	cryst	296					CAWSAW
NDI	cryst	150	69	2	150	293	alpha(300K)=69
PDI	cryst	263		4	263	295	
quinacridone	cryst	293	187	2	223	293	alpha(300K)=187
pentaceneN4O2	cryst	296					WUPYIQ
indigo	cryst	210		3	210	295	
indigoCl2	cryst	100					MOGSEI
dibenzoindigo	cryst	110					noCCDC
carbazoleNO2b	cryst	100					RITMAK
TTAa	cryst	100					VOBYAN
TTAb	cryst	100					VOBYER
TTPa	cryst	173					SESSOA
TTPb	cryst	173					SESTAN
TTPc	cryst	298					SESSUG
PBBTZ	cryst	113					MOJFEX
thiazolothiazolePh	cryst	293	170	2	100	293	alpha(300K)=170
benzodithiopheneO2	cryst	296					ZAPZAT
C60	cryst	5	83	13	5	298	V0=11.478(21)
triptycene	cryst	100	117	5	100	295	V0=9.83(5)
BODIPY	cryst	213	234	3	173	296	alpha(300K)=234
OPV3CN	cryst	173	186	2	173	293	alpha(300K)=186
spirobifluorene	cryst	293	162	3	115	295	alpha(300K)=162
spirobidibenzosilole	cryst	100					SIBMUN
triphenyltriazine	cryst	123	164	4	100	295	V0=9.37(4)
triphenylbenzene	cryst	100	165	5	100	296	V0=9.59(4)
TPP	cryst	90	192	10	90	299	V0=10.11(4)

Table S10: Comparison wrt experiment for V1 extrapolated to 0K [URL].

system	na1	no	ns	SG	V1	R2S	PBE	PBE*
anthracene	24	1	2	P21/c	9.34	-2.0	0.4	
anthraquinone	24	1	2	P21/c	9.62	-2.6	0.5	
benzene	12	1	2	Pbca	9.51	-2.7	0.4	
benzeneF6	12	2	1	P21/n	11.83	0.8	12.1	(excluded)
benzeneO2	12	1	2	P21/c	10.31	-1.4	3.7	(excluded)
BTBT	24	1	2	P21/c	10.91	-1.5	0.0	
C60	60	1	6	Pa-3	11.48	0.5	1.9	
carbazole	22	1	2	Pnma	9.16	-1.9	0.6	
chrysene	30	1	2	C12/n1	9.26	-0.9	1.3	
coronene	36	1	2	P21/n	9.53	-1.0	0.5	
DBTTF	26	1	2	P21/c	11.66	-0.6	0.2	
naphthalene	18	1	2	P21/c	9.38	-2.5	0.4	
pentacene	36	2	2	P-1	9.10	-1.3	0.8	
perylene	32	1	2	P21/c	9.19	-2.3	-0.3	
phenazine	22	1	2	P21/n	9.65	-1.6	1.0	
pyrene	26	1	1	P21/a	9.61	-1.8	-0.1	
spirobifluorene	41	1	1	P21/c	10.05	-1.4	0.5	
stilbene	26	2	2	P21/a	9.36	-2.1	0.1	
TCNQ	20	1	2	C2/c	12.31	-1.8	0.9	
TCNQ-F2	20	1	4	C2/m	12.32	-0.5	4.2	(excluded)
TCNQ-F4	20	1	2	Pbca	13.18	-0.4	5.5	(excluded)
tetracene	30	2	2	P-1	9.31	-2.3	-0.1	
TPP	34	1	1	P21/c	10.11	-2.1	-0.4	
triphenylbenzene	42	1	1	Pna21	9.59	-2.7	-0.4	
triphenylene	30	1	1	P212121	9.33	-2.9	-0.8	
triphenyltriazine	39	1	1	P21/c	9.37	-2.0	0.6	
triptycene	34	1	1	P212121	9.83	-2.7	-0.7	
TTF	14	1	2	P21/c	13.53	-0.1	-0.2	
median						-1.8	0.4	0.4
mean						-1.6	1.2	0.3
standard dev						1.0	2.6	0.6
lower decile						-2.7	-0.4	-0.5
upper decile						-0.1	4.1	1.1
min						-2.9	-0.8	-0.8
max						0.8	12.1	1.9

Table S11: Comparison experiment wrt R2SCAN-D3paw900 [URL].

system	na1	no	ns	SG	V1	dV1	dSh	dTv	da	db	dc	dalp	dbet	dgam	dr	phi	dev
str	#	#	#	str	Ao3	%	%	%	%	%	%	deg	deg	deg	mAo	deg	mAo
median						4.2	0.8	1.7	1.1	1.3	1.3	0.0	0.1	0.0	0	0.8	13
mean						4.1	1.0	1.9	1.2	1.5	1.4	0.0	0.1	-0.0	4	1.0	16
standard dev						1.8	0.6	0.9	0.9	1.2	1.0	0.2	0.8	0.0	9	0.7	10
lower decile						2.0	0.3	0.9	0.5	0.2	0.4	0.0	-0.7	0.0	0	0.3	7
upper decile						6.6	1.8	3.2	2.2	3.1	2.5	0.0	0.8	0.0	17	2.0	31
min						-0.1	0.0	0.0	-0.6	-0.8	-1.1	-0.9	-2.6	-0.3	0	0.0	3
max						8.1	2.7	4.6	4.5	4.4	5.3	1.1	2.0	0.1	41	3.1	44
anthracene	24	1	2	P21/c	9.15	3.9	0.4	1.5	1.3	0.9	1.8	0.0	0.3	0.0	0	1.0	9
anthraquinone	24	1	2	P21/c	9.37	5.0	0.6	1.9	1.0	2.6	1.4	0.0	0.1	0.0	0	1.1	9
benzene	12	1	2	Pbca	9.25	7.0	0.8	2.5	1.2	2.8	2.9	0.0	0.0	0.0	0	1.3	3
benzeneF6	12	2	1	P21/n	11.93	4.7	1.3	2.0	0.5	3.4	0.8	0.0	0.2	0.0	0	1.5	10
benzeneO2	12	1	2	P21/c	10.17	7.7	2.3	3.7	1.7	1.1	5.3	0.0	2.0	0.0	0	2.6	9
benzodithiopheneO2	18	1	2	P21/n	11.50	6.3	1.9	3.3	3.0	0.1	2.5	0.0	-2.3	0.0	0	2.8	41
benzotrithiophene	21	1	1	P21/n	12.27	5.4	2.7	3.2	0.7	-0.8	4.8	0.0	-1.1	0.0	41	3.1	44
benzotrithiopheneA	21	2	1	P21	12.00	2.1	0.3	1.0	0.9	0.6	0.7	0.0	0.3	0.0	17	0.2	12
bithiophene	16	1	2	P21/c	11.52	2.8	1.5	1.9	2.7	0.6	0.1	0.0	1.0	0.0	0	1.4	31
BODIPY	21	1	1	C2/c	9.50	8.1	1.1	2.6	1.9	4.1	1.8	0.0	-0.4	0.0	27	1.1	24
BTBT	24	1	2	P21/c	10.75	2.3	0.4	1.0	0.9	0.3	1.1	0.0	0.2	0.0	0	0.9	7
C60	60	1	6	Pa-3	11.53	0.0	0.0	0.0	0.0	0.0	0.0	0.0	0.0	0.0	0	0.2	20
carbazole	22	1	2	Pnma	8.98	4.2	0.3	1.6	1.8	1.2	1.2	0.0	0.0	0.0	18	0.9	6
carbazoleNO2b	24	1	1	P21/n	9.57	2.5	1.4	1.0	0.6	2.4	-0.4	0.0	0.5	0.0	24	0.7	11
chrysene	30	1	2	C12/n1	9.18	3.4	0.5	1.3	0.8	1.4	1.2	0.0	0.3	0.0	0	0.6	6
coronene	36	1	2	P21/n	9.43	2.4	0.3	0.9	1.1	0.7	0.5	0.0	0.0	0.0	0	0.2	6
DATT	48	1	1	P21	9.82	4.5	1.1	1.5	1.1	2.7	0.7	0.0	-0.1	0.0	9	1.2	15
DBTTF	26	1	2	P21/c	11.59	2.5	0.3	1.2	0.9	0.8	0.9	0.0	0.2	0.0	0	0.3	11
dibenzoindigo	42	1	2	P21/n	9.34	0.6	1.1	1.5	-0.6	0.8	0.4	0.0	-0.2	0.0	0	0.5	30
DNBDT	42	1	2	P21/n	9.79	4.7	0.8	1.9	0.7	2.5	1.6	0.0	0.4	0.0	0	0.9	18
DNTT	36	1	1	P21	10.21	4.4	0.9	1.7	0.6	2.8	0.9	0.0	0.2	0.0	17	1.3	19
hexacene	42	2	2	P-1	8.88	4.5	1.4	2.4	-0.2	3.5	1.4	1.1	-0.0	-0.1	0	2.1	31
HMTTF	28	1	1	P21/c	9.99	6.6	1.5	3.1	1.7	3.8	1.0	0.0	0.5	0.0	5	0.7	18
ICZb	32	1	2	P21/c	8.93	3.6	1.2	2.1	1.9	0.3	1.6	0.0	1.2	0.0	0	1.5	10
ICZbCl2c	32	1	2	P21/c	10.06	-0.1	0.9	0.9	0.6	0.6	-1.1	0.0	0.4	0.0	0	0.4	13
IF12b	34	1	2	P21/n	8.96	5.8	1.1	2.2	1.5	2.5	1.6	0.0	-1.3	0.0	0	0.7	8
IF21a	34	1	1	P21/c	9.36	4.2	0.9	2.2	-0.3	3.1	1.4	0.0	0.2	0.0	4	0.6	13
indigo	30	1	2	P21/n	9.34	3.6	0.8	1.7	2.2	0.2	1.3	0.0	0.3	0.0	0	0.5	9
indigoCl2	30	1	2	P21/c	10.72	1.7	1.0	1.1	-0.3	1.4	1.0	0.0	0.6	0.0	0	0.8	7
naphthalene	18	1	2	P21/c	9.15	4.0	0.6	1.7	1.7	0.9	1.7	0.0	0.5	0.0	0	1.1	3
NDFPh	44	1	2	P21/c	9.56	7.3	1.3	2.6	1.6	4.4	1.3	0.0	0.4	0.0	0	1.6	18
NDI	26	2	2	P-1	9.68	3.3	0.8	1.3	1.1	1.3	0.6	0.7	0.6	-0.3	0	0.3	10
NDT	24	2	2	P21/c	10.75	7.2	2.2	4.6	4.5	0.8	1.7	0.0	-0.3	0.0	0	2.1	38
oligothiophene4	30	1	2	P21/a	11.55	5.5	2.4	3.2	0.7	1.6	2.5	0.0	-2.6	0.0	0	2.5	25
oligothiophene6	44	1	2	P21/a	11.53	4.9	1.9	3.4	1.5	1.2	2.5	0.0	1.9	0.0	0	1.7	26
OPV3CN	42	1	2	Pbca	9.88	4.7	0.6	2.2	1.0	2.4	1.2	0.0	0.0	0.0	0	1.0	38
PBBTZ	30	1	1	P21/n	10.44	1.9	0.7	0.6	1.0	0.1	0.8	0.0	-0.4	0.0	8	0.4	10
PDI	40	1	2	P21/n	9.35	3.4	0.6	1.4	0.9	0.9	1.6	0.0	0.8	0.0	0	0.4	25
pentacene	36	2	2	P-1	8.98	4.7	0.9	2.1	0.9	2.6	1.5	-0.9	-0.1	0.1	0	1.3	13
pentaceneN2Cl4	34	1	2	P21/n	11.61	2.4	0.5	0.7	1.5	0.4	0.4	0.0	-0.2	0.0	0	0.7	12
pentaceneN4O2	32	1	2	P21/n	9.62	5.6	1.4	1.7	3.8	0.7	1.0	0.0	-0.7	0.0	0	1.2	14
perylene	32	1	2	P21/c	8.98	4.6	0.8	1.4	1.3	2.6	0.6	0.0	-0.2	0.0	0	0.3	12
phenazine	22	1	2	P21/n	9.50	7.2	1.5	3.4	0.8	2.6	3.2	0.0	-1.2	0.0	0	1.4	10
PTCDA	38	1	2	P21/c	9.73	2.4	0.8	0.7	1.6	0.2	0.7	0.0	0.6	0.0	0	0.5	30
pyrene	26	1	1	P21/a	9.43	3.6	0.4	1.2	0.6	1.4	1.4	0.0	-0.1	0.0	16	0.4	7
quinacridone	36	1	2	P21/c	9.22	5.5	1.5	2.8	1.7	2.3	1.9	0.0	1.4	0.0	0	2.1	43
spirobidibenzosilole	41	1	2	P41212	10.25	3.6	0.3	1.3	1.3	1.3	0.9	0.0	0.0	0.0	32	0.8	22
spirobifluorene	41	1	1	P21/c	9.92	6.5	0.6	2.4	1.3	2.5	2.5	0.0	-0.4	0.0	14	0.4	22
stilbene	26	2	2	P21/a	9.16	4.3	0.2	1.6	1.2	1.7	1.4	0.0	-0.1	0.0	0	0.8	14
TCNQ	20	1	2	C2/c	12.08	3.7	1.3	1.2	0.9	2.8	0.0	0.0	0.4	0.0	0	0.6	12
TCNQ-F2	20	1	4	C2/m	12.26	4.2	1.0	1.4	0.6	3.0	0.6	0.0	0.2	0.0	0	0.0	12
TCNQ-F4	20	1	2	Pbca	13.13	4.2	0.3	1.6	1.8	0.8	1.5	0.0	0.0	0.0	0	0.6	13
tetracene	30	2	2	P-1	9.10	4.9	0.8	2.0	1.1	2.5	1.4	-0.7	0.3	0.0	0	1.3	13
thiazolothiazolePh	30	1	2	P21/c	10.49	6.1	0.8	3.0	2.1	1.7	1.8	0.0	-1.1	0.0	0	1.1	21
TPP	34	1	1	P21/c	9.89	3.8	0.7	1.5	0.8	0.9	2.1	0.0	0.6	0.0	13	0.6	14
triazine	9	1	2	C2/c	9.80	4.2	1.9	2.7	4.1	1.0	1.2	0.0	1.8	0.0	9	1.9	3
triphenylbenzene	42	1	1	Pna21	9.33	4.5	0.9	1.3	2.8	0.7	0.9	0.0	0.0	0.0	7	0.5	38
triphenylene	30	1	1	P212121	9.06	4.7	0.2	1.9	1.4	1.8	1.4	0.0	0.0	0.0	9	0.3	10
triphenyltriazine	39	1	1	P21/c	9.18	4.5	0.8	2.1	1.2	2.2	1.1	0.0	0.0	0.0	9	0.3	13
triptycene	34	1	1	P212121	9.57	4.3	0.0	1.7	1.4	1.5	1.4	0.0	0.0	0.0	12	0.2	15
TTAa	36	1	2	P21/n	11.13	1.3	0.6	1.0	0.7	-0.3	0.9	0.0	-0.3	0.0	0	0.5	13
TTAb	36	1	2	P21/n	11.14	2.9	0.9	1.6	0.5	0.5	1.9	0.0	0.1	0.0	0	0.4	16
TTF	14	1	2	P21/c	13.52	6.3	0.9	2.3	1.4	3.4	1.7	0.0	0.7	0.0	0	0.7	9
TTPa	34	1	2	P21/n	11.51	2.1	0.4	1.0	0.9	0.3	0.9	0.0	-0.4	0.0	0	0.4	11
TTPb	34	2	2	P21/a	11.67	1.9	0.6	0.6	0.7	1.1	0.2	0.0	0.1	0.0	0	1.1	20
TTPc	34	1	1	P21	11.76	3.5	1.7	2.6	0.7	-0.4	3.0	0.0	-0.5	0.0	8	1.2	18
TTTT	18	1	2	P21/n	12.57	3.4	0.7	1.2	0.3	1.8	1.3	0.0	0.2	0.0	0	0.6	7

Table S12: Comparison experiment wrt PBE-D3paw900 [URL].

system	na1	no	ns	SG	V1	dV1	dSh	dTv	da	db	dc	dalp	dbet	dgam	dr	phi	dev
str	#	#	#	str	Ao3	%	%	%	%	%	%	deg	deg	deg	mAo	deg	mAo
median						1.8	0.7	1.0	0.5	0.7	0.5	0.0	0.0	0.0	0	0.6	18
mean						1.6	0.8	1.2	0.5	0.7	0.4	-0.0	0.0	0.0	4	0.8	20
standard dev						2.0	0.6	0.8	0.9	1.0	1.0	0.1	0.5	0.1	7	0.6	11
lower decile						-1.2	0.2	0.5	-0.5	-0.5	-0.9	0.0	-0.5	0.0	0	0.2	9
upper decile						4.0	1.5	2.2	1.4	1.9	1.6	0.0	0.7	0.0	13	1.7	37
min						-5.8	0.0	0.2	-2.2	-3.0	-3.3	-0.3	-1.9	-0.5	0	0.1	3
max						6.4	3.1	4.6	4.7	3.5	2.9	0.4	1.3	0.3	37	2.6	52
anthracene	24	1	2	P21/c	9.38	1.4	0.3	0.5	0.3	1.0	0.2	0.0	0.1	0.0	0	0.4	8
anthraquinone	24	1	2	P21/c	9.67	1.8	0.9	0.5	0.6	1.4	-0.2	0.0	0.0	0.0	0	0.7	12
benzene	12	1	2	Pbca	9.54	3.7	0.1	1.3	1.2	1.4	1.1	0.0	0.0	0.0	0	0.5	3
benzeneF6	12	2	1	P21/n	13.26	-5.8	0.7	2.5	-1.1	-3.0	-1.8	0.0	-0.1	0.0	0	1.0	21
benzeneO2	12	1	2	P21/c	10.70	2.4	1.3	1.7	-0.6	2.2	1.1	0.0	1.0	0.0	0	2.2	14
benzodithiopheneO2	18	1	2	P21/n	11.82	3.4	0.5	1.2	1.9	0.6	0.9	0.0	-0.3	0.0	0	0.8	40
benzotrithiophene	21	1	1	P21/n	12.45	4.0	1.4	1.9	0.5	0.2	2.9	0.0	-0.4	0.0	12	1.7	48
benzotrithiopheneA	21	2	1	P21	12.11	1.1	0.2	0.5	0.6	0.2	0.4	0.0	0.1	0.0	37	0.4	13
bithiophene	16	1	2	P21/c	11.72	1.1	1.5	1.5	1.7	0.9	-1.3	0.0	0.5	0.0	0	1.8	32
BODIPY	21	1	1	C2/c	9.97	3.0	0.8	1.5	-0.1	1.3	1.6	0.0	-0.4	0.0	8	1.0	25
BTBT	24	1	2	P21/c	10.91	0.7	0.6	0.7	0.1	-0.4	1.1	0.0	0.2	0.0	0	1.1	8
C60	60	1	6	Pa-3	11.70	-1.4	0.0	0.5	-0.5	-0.5	-0.5	0.0	0.0	0.0	0	0.2	18
carbazole	22	1	2	Pnma	9.21	1.6	0.1	0.6	0.6	0.4	0.6	0.0	0.0	0.0	8	0.2	10
carbazoleNO2b	24	1	1	P21/n	9.96	-1.5	1.3	1.6	-0.8	0.9	-1.2	0.0	1.0	0.0	30	1.2	19
chrysene	30	1	2	C12/n1	9.38	1.1	0.8	0.6	-0.1	1.3	0.1	0.0	0.5	0.0	0	0.3	11
coronene	36	1	2	P21/n	9.57	0.9	0.6	0.9	0.5	-0.4	0.8	0.0	-0.0	0.0	0	0.1	10
DATT	48	1	1	P21	9.98	2.8	0.9	0.9	1.0	1.5	0.2	0.0	-0.5	0.0	15	0.7	24
DBTTF	26	1	2	P21/c	11.69	1.7	0.4	0.9	0.7	0.6	0.6	0.0	0.3	0.0	0	0.1	13
dibenzoindigo	42	1	2	P21/n	9.59	-2.0	3.1	2.1	-2.2	1.1	-0.9	0.0	0.7	0.0	0	1.7	52
DNBDT	42	1	2	P21/n	9.94	3.1	0.6	1.3	0.5	1.7	1.0	0.0	0.3	0.0	0	0.7	11
DNTT	36	1	1	P21	10.39	2.6	0.7	0.9	0.8	1.5	0.3	0.0	0.4	0.0	9	0.7	30
hexacene	42	2	2	P-1	9.05	2.5	1.2	1.8	-0.8	2.1	1.2	0.4	-1.0	-0.5	0	1.7	25
HMTTF	28	1	1	P21/c	10.18	4.7	1.8	2.8	1.1	3.5	0.1	0.0	0.3	0.0	12	0.2	18
ICZb	32	1	2	P21/c	9.16	1.0	0.2	0.4	0.3	0.5	0.3	0.0	0.3	0.0	0	0.4	11
ICZbCl2c	32	1	2	P21/c	10.34	-2.8	1.6	1.7	-0.1	0.6	-3.3	0.0	-0.2	0.0	0	1.7	24
IF12b	34	1	2	P21/n	9.17	3.4	1.0	1.8	0.5	1.3	1.5	0.0	-1.0	0.0	0	0.8	16
IF21a	34	1	1	P21/c	9.58	1.8	0.6	0.6	0.7	0.9	0.2	0.0	0.3	0.0	10	0.6	10
indigo	30	1	2	P21/n	9.59	0.9	0.4	0.6	0.6	-0.2	0.6	0.0	0.0	0.0	0	0.2	22
indigoCl2	30	1	2	P21/c	11.01	-0.9	1.3	1.5	-1.6	1.0	-0.5	0.0	-0.3	0.0	0	1.7	20
naphthalene	18	1	2	P21/c	9.41	1.1	0.2	0.4	0.2	0.6	0.4	0.0	0.1	0.0	0	0.4	7
NDFPh	44	1	2	P21/c	9.86	4.0	0.9	1.4	0.7	2.2	1.2	0.0	0.5	0.0	0	1.0	23
NDI	26	2	2	P-1	10.07	-0.7	1.2	1.3	1.4	-0.6	-1.4	-0.2	-0.3	0.2	0	1.3	13
NDT	24	2	2	P21/c	10.92	5.6	2.9	4.6	4.7	-0.0	0.8	0.0	-0.6	0.0	0	2.6	39
oligothiophene4	30	1	2	P21/a	11.73	3.8	1.9	2.3	-0.2	1.8	1.7	0.0	-1.9	0.0	0	1.8	31
oligothiophene6	44	1	2	P21/a	11.70	3.3	1.2	2.2	0.6	1.4	1.5	0.0	1.3	0.0	0	0.9	32
OPV3CN	42	1	2	Pbca	10.12	2.2	1.0	0.6	0.7	1.4	0.1	0.0	0.0	0.0	0	0.4	50
PBBTZ	30	1	1	P21/n	10.57	0.7	0.6	0.5	-0.1	-0.1	0.8	0.0	-0.3	0.0	13	0.5	21
PDI	40	1	2	P21/n	9.64	0.2	0.8	0.8	0.8	-0.8	0.2	0.0	0.2	0.0	0	1.0	27
pentacene	36	2	2	P-1	9.17	2.6	0.7	1.4	0.4	1.2	1.1	-0.3	-0.8	0.3	0	0.9	9
pentaceneN2Cl4	34	1	2	P21/n	11.88	0.1	0.8	0.8	-0.1	0.7	-0.5	0.0	-0.1	0.0	0	0.5	11
pentaceneN4O2	32	1	2	P21/n	9.92	2.4	1.0	0.7	2.2	0.1	0.2	0.0	0.7	0.0	0	1.5	17
perylene	32	1	2	P21/c	9.16	2.5	1.8	1.6	0.2	3.0	-0.9	0.0	-0.9	0.0	0	0.8	17
phenazine	22	1	2	P21/n	9.75	4.5	0.5	2.0	1.7	0.8	1.8	0.0	-0.2	0.0	0	2.0	18
PTCDA	38	1	2	P21/c	10.10	-1.3	0.6	1.1	0.1	-0.9	-0.5	0.0	-0.4	0.0	0	0.4	37
pyrene	26	1	1	P21/a	9.60	1.7	0.9	1.0	-0.4	1.5	0.6	0.0	-0.3	0.0	11	0.9	12
quinacridone	36	1	2	P21/c	9.47	2.7	1.3	1.8	1.1	0.9	1.0	0.0	1.1	0.0	0	1.0	45
spirobidibenzosilole	41	1	2	P41212	10.43	1.8	0.2	0.9	0.5	0.5	0.8	0.0	0.0	0.0	5	0.4	18
spirobifluorene	41	1	1	P21/c	10.11	4.4	0.4	1.7	0.8	1.9	1.6	0.0	-0.2	0.0	15	0.4	23
stilbene	26	2	2	P21/a	9.37	2.0	0.4	0.9	1.1	0.7	0.4	0.0	0.2	0.0	0	0.5	10
TCNQ	20	1	2	C2/c	12.42	0.8	1.0	0.9	0.4	1.1	-0.5	0.0	0.8	0.0	0	1.3	17
TCNQ-F2	20	1	4	C2/m	12.84	-0.5	0.5	0.5	-0.0	-0.5	0.2	0.0	0.5	0.0	0	0.2	17
TCNQ-F4	20	1	2	Pbca	13.90	-1.7	1.2	1.1	-1.2	-1.3	0.8	0.0	0.0	0.0	0	0.8	21
tetracene	30	2	2	P-1	9.30	2.7	0.3	1.1	1.0	1.0	0.9	-0.1	-0.3	0.2	0	0.3	11
thiazolothiazolePh	30	1	2	P21/c	10.70	4.0	0.5	2.4	1.1	1.1	1.5	0.0	-0.4	0.0	0	1.1	21
TPP	34	1	1	P21/c	10.07	2.0	1.0	1.1	0.5	-0.2	1.7	0.0	0.6	0.0	21	0.1	26
triazine	9	1	2	C2/c	10.20	0.0	0.5	0.5	0.4	0.1	-0.7	0.0	-0.2	0.0	4	0.4	5
triphenylbenzene	42	1	1	Pna21	9.55	2.2	0.6	0.7	1.6	0.3	0.3	0.0	0.0	0.0	3	0.3	25
triphenylene	30	1	1	P212121	9.25	2.5	0.4	1.2	0.7	0.6	1.2	0.0	0.0	0.0	15	0.3	11
triphenyltriazine	39	1	1	P21/c	9.43	1.8	0.2	1.0	0.6	0.6	0.5	0.0	-0.1	0.0	11	0.1	12
triptycene	34	1	1	P212121	9.77	2.2	0.2	0.7	0.7	1.0	0.5	0.0	0.0	0.0	7	0.1	4
TTAa	36	1	2	P21/n	11.27	0.1	0.2	0.2	-0.0	-0.0	0.1	0.0	0.2	0.0	0	0.3	19
TTAb	36	1	2	P21/n	11.25	1.9	0.4	0.8	0.2	0.7	0.9	0.0	-0.2	0.0	0	0.2	10
TTF	14	1	2	P21/c	13.51	6.4	0.7	2.8	1.3	2.9	2.3	0.0	0.5	0.0	0	1.2	14
TTPa	34	1	2	P21/n	11.67	0.6	0.5	0.5	0.2	0.4	0.1	0.0	0.5	0.0	0	0.4	16
TTPb	34	2	2	P21/a	11.83	0.6	0.5	0.6	0.6	0.2	-0.1	0.0	0.2	0.0	0	0.6	29
TTPc	34	1	1	P21	11.92	2.0	0.9	1.4	0.3	0.1	1.6	0.0	-0.2	0.0	8	0.4	18
TTTT	18	1	2	P21/n	12.70	2.3	0.7	0.7	0.0	1.6	0.7	0.0	0.0	0.0	0	0.6	16

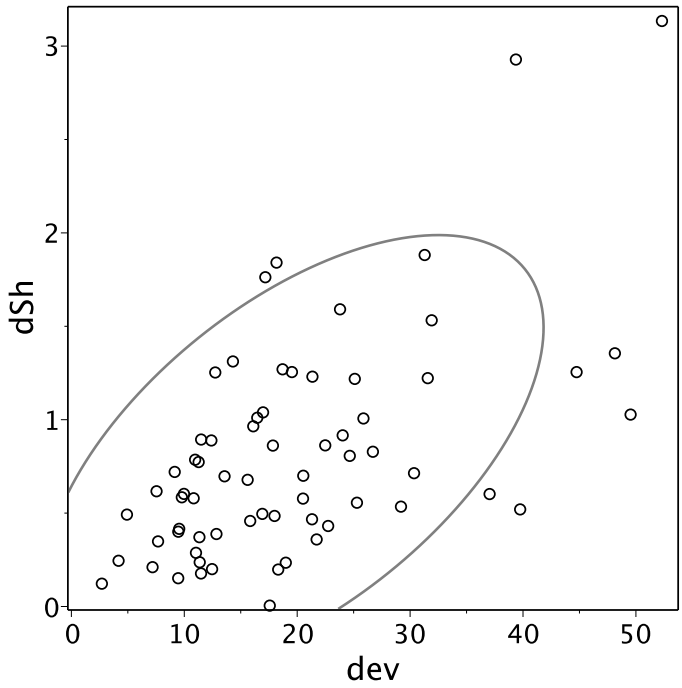

Figure S3: Comparison experiment wrt PBE-D3paw900: dev-dSh correlation [URL].

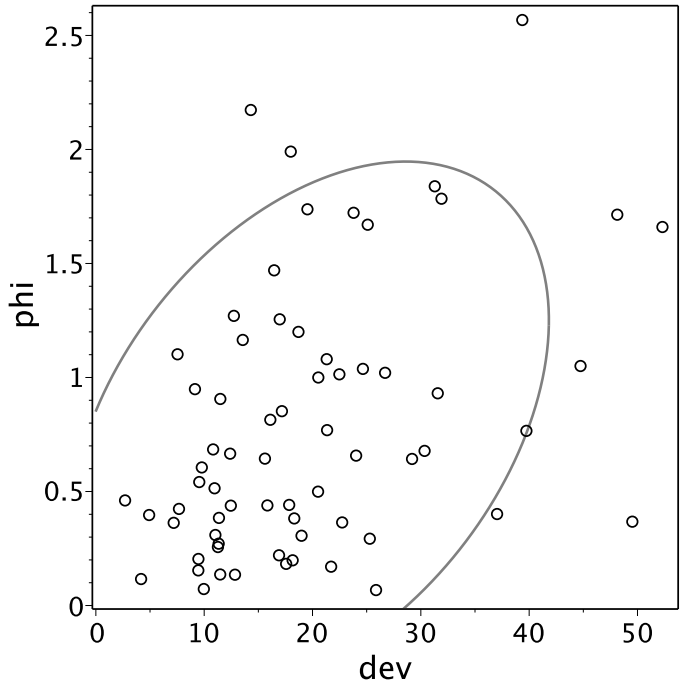

Figure S4: Comparison experiment wrt PBE-D3paw900: dev-phi correlation [URL].

Table S13: Comparison R2SCAN wrt PBE-D3 [URL].

system	na1	no	ns	SG	V1	dV1	dSh	dTv	da	db	dc	dalp	dbet	dgam	dr	phi	dev
str	#	#	#	str	Ao3	%	%	%	%	%	%	deg	deg	deg	mAo	deg	mAo
median						-2.2	0.7	1.1	-0.7	-0.7	-0.9	0.0	-0.0	0.0	0	0.8	16
mean						-2.4	0.8	1.2	-0.8	-0.8	-0.9	-0.0	-0.0	0.0	5	0.9	16
standard dev						1.4	0.5	0.6	0.8	1.1	0.7	0.2	0.6	0.1	10	0.6	5
lower decile						-3.9	0.3	0.6	-1.6	-1.8	-1.8	0.0	-0.8	0.0	0	0.2	10
upper decile						-1.3	1.4	1.9	-0.0	0.3	-0.2	0.0	0.7	0.0	20	1.6	23
min						-10.1	0.0	0.4	-3.5	-6.2	-4.0	-1.0	-1.9	-0.3	0	0.0	5
max						0.1	2.3	4.3	1.0	1.1	0.6	0.6	2.1	0.5	52	2.5	28
anthracene	24	1	2	P21/c	9.38	-2.4	0.7	1.2	-1.1	0.1	-1.6	0.0	-0.2	0.0	0	1.3	10
anthraquinone	24	1	2	P21/c	9.67	-3.1	0.6	1.8	-0.5	-1.2	-1.5	0.0	-0.1	0.0	0	0.9	12
benzene	12	1	2	Pbca	9.54	-3.1	0.7	1.3	0.0	-1.4	-1.8	0.0	0.0	0.0	0	1.5	5
benzeneF6	12	2	1	P21/n	13.26	-10.1	1.9	4.3	-1.6	-6.2	-2.6	0.0	-0.2	0.0	0	2.5	13
benzeneO2	12	1	2	P21/c	10.70	-4.9	2.3	2.9	-2.2	1.1	-4.0	0.0	-0.9	0.0	0	2.1	10
benzodithiopheneO2	18	1	2	P21/n	11.82	-2.7	1.8	2.3	-1.0	0.5	-1.6	0.0	2.1	0.0	0	2.3	11
benzotrithiophene	21	1	1	P21/n	12.45	-1.4	1.4	1.4	-0.2	1.0	-1.8	0.0	0.6	0.0	30	1.4	12
benzotrithiopheneA	21	2	1	P21	12.11	-0.9	0.2	0.4	-0.3	-0.4	-0.4	0.0	-0.2	0.0	20	0.6	12
bithiophene	16	1	2	P21/c	11.72	-1.7	0.8	1.2	-1.0	0.4	-1.3	0.0	-0.5	0.0	0	1.5	9
BODIPY	21	1	1	C2/c	9.97	-4.7	1.3	1.6	-1.9	-2.7	-0.2	0.0	-0.0	0.0	28	1.6	12
BTBT	24	1	2	P21/c	10.91	-1.5	0.4	0.8	-0.8	-0.7	0.0	0.0	-0.0	0.0	0	0.3	12
C60	60	1	6	Pa-3	11.70	-1.4	0.0	0.5	-0.5	-0.5	-0.5	0.0	0.0	0.0	0	0.0	15
carbazole	22	1	2	Pnma	9.21	-2.5	0.2	1.0	-1.2	-0.7	-0.6	0.0	0.0	0.0	19	1.1	11
carbazoleNO2b	24	1	1	P21/n	9.96	-3.9	0.6	1.4	-1.4	-1.5	-0.9	0.0	0.5	0.0	52	0.8	13
chrysene	30	1	2	C12/n1	9.38	-2.2	0.4	1.3	-0.9	-0.1	-1.1	0.0	0.1	0.0	0	0.3	11
coronene	36	1	2	P21/n	9.57	-1.5	0.8	0.6	-0.6	-1.1	0.3	0.0	-0.1	0.0	0	0.3	12
DATT	48	1	1	P21	9.98	-1.7	0.4	0.8	-0.0	-1.2	-0.4	0.0	-0.4	0.0	7	0.7	23
DBTTF	26	1	2	P21/c	11.69	-0.8	0.1	0.4	-0.2	-0.2	-0.3	0.0	0.1	0.0	0	0.2	15
dibenzoindigo	42	1	2	P21/n	9.59	-2.6	2.1	0.9	-1.6	0.3	-1.3	0.0	0.8	0.0	0	1.3	24
DNBDT	42	1	2	P21/n	9.94	-1.5	0.3	0.7	-0.2	-0.8	-0.6	0.0	-0.1	0.0	0	0.3	19
DNTT	36	1	1	P21	10.39	-1.7	0.4	0.9	0.2	-1.3	-0.6	0.0	0.2	0.0	10	0.7	18
hexacene	42	2	2	P-1	9.05	-2.0	1.0	1.2	-0.6	-1.4	-0.3	-0.7	-1.0	-0.3	0	1.6	18
HMTTF	28	1	1	P21/c	10.18	-1.9	0.3	0.7	-0.7	-0.3	-0.9	0.0	-0.2	0.0	16	0.5	15
ICZb	32	1	2	P21/c	9.16	-2.5	1.1	1.8	-1.6	0.2	-1.3	0.0	-0.9	0.0	0	1.8	16
ICZbCl2c	32	1	2	P21/c	10.34	-2.7	0.9	1.4	-0.7	0.0	-2.2	0.0	-0.6	0.0	0	1.7	17
IF12b	34	1	2	P21/n	9.17	-2.2	0.7	0.7	-1.0	-1.1	-0.1	0.0	0.3	0.0	0	0.1	15
IF21a	34	1	1	P21/c	9.58	-2.3	1.1	1.8	1.0	-2.1	-1.2	0.0	0.1	0.0	12	1.1	19
indigo	30	1	2	P21/n	9.59	-2.6	0.6	1.2	-1.6	-0.4	-0.7	0.0	-0.3	0.0	0	0.4	19
indigoCl2	30	1	2	P21/c	11.01	-2.6	1.1	1.8	-1.3	-0.4	-1.4	0.0	-0.9	0.0	0	1.6	22
naphthalene	18	1	2	P21/c	9.41	-2.8	0.6	1.3	-1.6	-0.3	-1.2	0.0	-0.3	0.0	0	1.0	8
NDFPh	44	1	2	P21/c	9.86	-3.0	0.6	1.3	-0.9	-2.0	-0.1	0.0	0.1	0.0	0	0.7	24
NDI	26	2	2	P-1	10.07	-3.8	1.5	2.0	0.3	-1.8	-2.1	-1.0	-1.0	0.5	0	1.5	18
NDT	24	2	2	P21/c	10.92	-1.5	0.7	0.6	0.1	-0.8	-0.9	0.0	-0.2	0.0	0	0.6	11
oligothiophene4	30	1	2	P21/a	11.73	-1.6	0.7	1.0	-0.8	0.2	-0.8	0.0	0.7	0.0	0	1.0	17
oligothiophene6	44	1	2	P21/a	11.70	-1.5	0.8	1.3	-0.9	0.2	-0.9	0.0	-0.6	0.0	0	1.1	25
OPV3CN	42	1	2	Pbca	10.12	-2.4	0.5	1.9	-0.4	-1.0	-1.1	0.0	0.0	0.0	0	0.7	26
PBBTZ	30	1	1	P21/n	10.57	-1.3	0.4	0.4	-1.0	-0.2	0.0	0.0	0.1	0.0	12	0.2	16
PDI	40	1	2	P21/n	9.64	-3.1	0.7	1.8	-0.1	-1.6	-1.4	0.0	-0.5	0.0	0	1.1	23
pentacene	36	2	2	P-1	9.17	-2.0	0.8	1.1	-0.5	-1.4	-0.4	0.5	-0.7	0.2	0	1.4	16
pentaceneN2Cl4	34	1	2	P21/n	11.88	-2.3	0.8	1.1	-1.6	0.3	-1.0	0.0	0.1	0.0	0	0.7	16
pentaceneN4O2	32	1	2	P21/n	9.92	-3.0	0.7	1.3	-1.6	-0.6	-0.9	0.0	1.4	0.0	0	1.1	19
perylene	32	1	2	P21/c	9.16	-2.0	1.0	1.5	-1.1	0.4	-1.5	0.0	-0.6	0.0	0	0.6	10
phenazine	22	1	2	P21/n	9.75	-2.6	1.4	1.7	0.9	-1.7	-1.4	0.0	1.0	0.0	0	1.1	10
PTCDA	38	1	2	P21/c	10.10	-3.6	0.4	1.6	-1.5	-1.1	-1.2	0.0	-0.9	0.0	0	0.4	22
pyrene	26	1	1	P21/a	9.60	-1.8	0.5	0.9	-1.0	0.1	-0.8	0.0	-0.2	0.0	20	0.8	10
quinacridone	36	1	2	P21/c	9.47	-2.7	0.4	1.0	-0.6	-1.3	-0.9	0.0	-0.3	0.0	0	1.2	17
spirobidibenzosilole	41	1	2	P41212	10.43	-1.8	0.5	0.5	-0.8	-0.8	-0.2	0.0	0.0	0.0	27	0.4	25
spirobifluorene	41	1	1	P21/c	10.11	-1.9	0.3	0.8	-0.5	-0.5	-0.9	0.0	0.2	0.0	6	0.3	13
stilbene	26	2	2	P21/a	9.37	-2.2	0.6	1.0	-0.1	-1.0	-1.0	0.0	0.3	0.0	0	0.4	14
TCNQ	20	1	2	C2/c	12.42	-2.7	0.6	0.9	-0.5	-1.6	-0.6	0.0	0.4	0.0	0	0.7	18
TCNQ-F2	20	1	4	C2/m	12.84	-4.5	1.3	1.6	-0.6	-3.4	-0.4	0.0	0.3	0.0	0	0.2	18
TCNQ-F4	20	1	2	Pbca	13.90	-5.6	1.2	1.9	-2.9	-2.1	-0.7	0.0	0.0	0.0	0	0.9	19
tetracene	30	2	2	P-1	9.30	-2.1	0.8	1.1	-0.1	-1.4	-0.5	0.6	-0.5	0.1	0	1.2	13
thiazolothiazolePh	30	1	2	P21/c	10.70	-2.0	0.7	0.7	-1.0	-0.5	-0.3	0.0	0.7	0.0	0	1.0	18
TPP	34	1	1	P21/c	10.07	-1.8	0.5	0.9	-0.3	-1.2	-0.3	0.0	-0.0	0.0	23	0.7	28
triazine	9	1	2	C2/c	10.20	-4.0	1.8	2.6	-3.5	-0.9	-1.9	0.0	-1.9	0.0	5	1.5	6
triphenylbenzene	42	1	1	Pna21	9.55	-2.2	0.4	0.7	-1.2	-0.4	-0.6	0.0	0.0	0.0	6	0.2	22
triphenylene	30	1	1	P212121	9.25	-2.1	0.6	0.9	-0.7	-1.2	-0.2	0.0	0.0	0.0	13	0.3	11
triphenyltriazine	39	1	1	P21/c	9.43	-2.6	0.6	1.1	-0.6	-1.5	-0.6	0.0	-0.1	0.0	9	0.2	17
triptycene	34	1	1	P212121	9.77	-2.0	0.2	1.0	-0.7	-0.5	-0.9	0.0	0.0	0.0	8	0.1	12
TTAa	36	1	2	P21/n	11.27	-1.2	0.7	1.0	-0.7	0.3	-0.8	0.0	0.6	0.0	0	0.7	17
TTAb	36	1	2	P21/n	11.25	-1.0	0.6	0.8	-0.2	0.2	-1.0	0.0	-0.2	0.0	0	0.4	16
TTF	14	1	2	P21/c	13.51	0.1	0.6	0.6	-0.0	-0.5	0.6	0.0	-0.2	0.0	0	0.9	8
TTPa	34	1	2	P21/n	11.67	-1.4	0.9	1.1	-0.7	0.1	-0.7	0.0	0.8	0.0	0	0.8	16
TTPb	34	2	2	P21/a	11.83	-1.3	0.4	0.4	-0.1	-0.9	-0.3	0.0	0.2	0.0	0	0.6	17
TTPc	34	1	1	P21	11.92	-1.4	0.9	1.2	-0.4	0.5	-1.4	0.0	0.3	0.0	6	0.8	18
TTTT	18	1	2	P21/n	12.70	-1.0	0.3	0.6	-0.3	-0.2	-0.6	0.0	-0.2	0.0	0	0.2	11

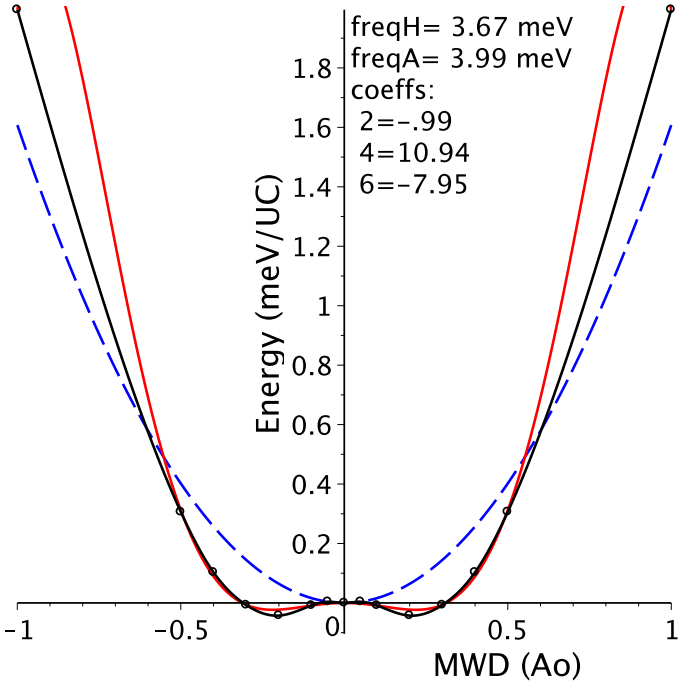

Figure S5: PES scans of imaginary frequencies: benzeneO2 by PBE-D3 [URL].

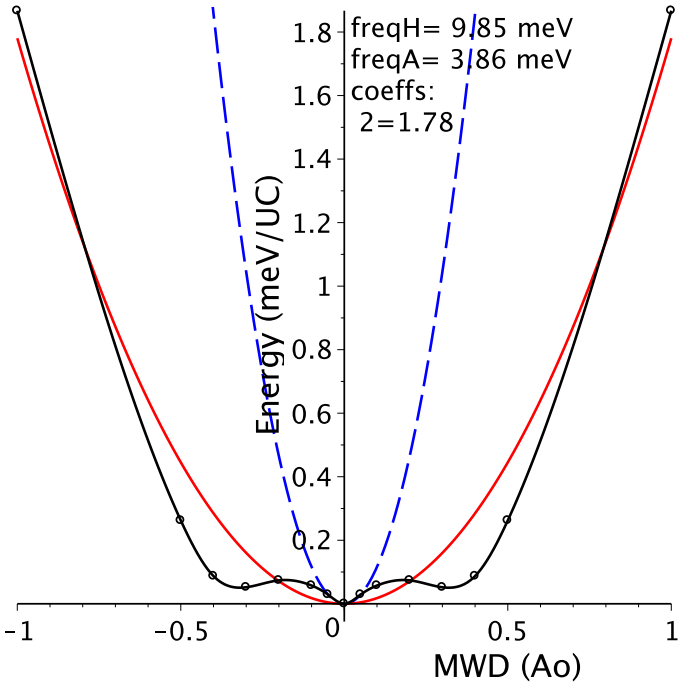

Figure S6: PES scans of imaginary frequencies: carbazoleNO2b by PBE-D3 [URL].

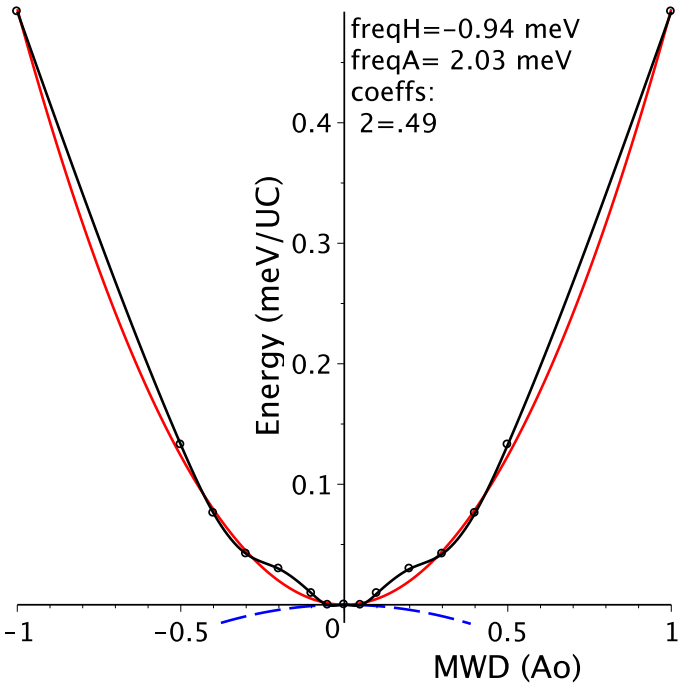

Figure S7: PES scans of imaginary frequencies: IF21a by PBE-D3 [URL].

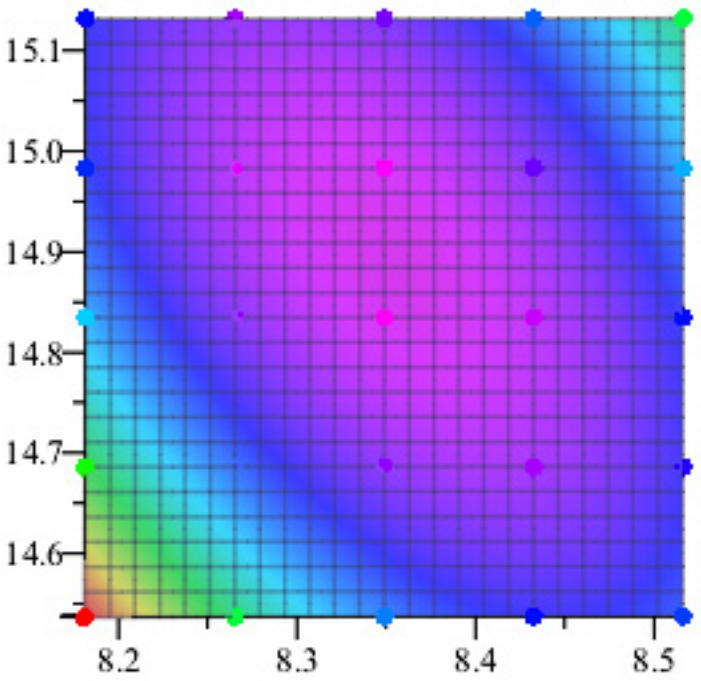

Figure S8: PES scans of unit cell parameters: TPP 2D scan in ab-plane plane by PBE-D3 [URL].

Table S14: PES scans of unit cell parameters: TPP 2D scan in ab-plane plane by PBE-D3 [URL].

2D cg2-scan of cryst_PBE-D3paw900 (opttol=1e-3):

x1	x2	E	V1	a	b	c	alp	bet	gam	dE	res(ueV)	file
8.1820	14.5380	-6.60770	9.6748	8.182	14.538	11.063	90.000	90.919	90.000	757	-7	11
8.1820	14.6863	-6.60799	9.7735	8.182	14.686	11.063	90.000	90.919	90.000	471	-1	12
8.1820	14.8346	-6.60817	9.8722	8.182	14.835	11.063	90.000	90.919	90.000	284	-6	13
8.1820	14.9830	-6.60827	9.9710	8.182	14.983	11.063	90.000	90.919	90.000	185	-9	14
8.1820	15.1313	-6.60829	10.0697	8.182	15.131	11.063	90.000	90.919	90.000	168	-3	15
8.2655	14.5380	-6.60803	9.7735	8.265	14.538	11.063	90.000	90.928	90.000	425	8	21
8.2655	14.6863	-6.60825	9.8733	8.265	14.686	11.063	90.000	90.928	90.000	204	15	22
8.2655	14.8346	-6.60838	9.9730	8.265	14.835	11.063	90.000	90.928	90.000	79	10	23
8.2655	14.9830	-6.60842	10.0727	8.265	14.983	11.063	90.000	90.928	90.000	34	8	24
8.2655	15.1313	-6.60839	10.1724	8.265	15.131	11.063	90.000	90.928	90.000	68	11	25
8.3490	14.5380	-6.60822	9.8722	8.349	14.538	11.063	90.000	90.938	90.000	237	-2	31
8.3490	14.6863	-6.60838	9.9730	8.349	14.686	11.063	90.000	90.938	90.000	79	4	32
8.3490	14.8346	-6.60845	10.0737	8.349	14.835	11.063	90.000	90.938	90.000	9	-1	33
8.3490	14.9830	-6.60844	10.1745	8.349	14.983	11.063	90.000	90.938	90.000	16	-4	34
8.3490	15.1313	-6.60836	10.2752	8.349	15.131	11.063	90.000	90.938	90.000	94	1	35
8.4324	14.5380	-6.60829	9.9710	8.432	14.538	11.063	90.000	90.947	90.000	170	-12	41
8.4324	14.6863	-6.60839	10.0727	8.432	14.686	11.063	90.000	90.947	90.000	67	-6	42
8.4324	14.8346	-6.60841	10.1745	8.432	14.835	11.063	90.000	90.947	90.000	47	-10	43
8.4324	14.9830	-6.60836	10.2762	8.432	14.983	11.063	90.000	90.947	90.000	100	-13	44
8.4324	15.1313	-6.60824	10.3779	8.432	15.131	11.063	90.000	90.947	90.000	219	-7	45
8.5159	14.5380	-6.60826	10.0697	8.516	14.538	11.063	90.000	90.957	90.000	198	3	51
8.5159	14.6863	-6.60831	10.1724	8.516	14.686	11.063	90.000	90.957	90.000	143	9	52
8.5159	14.8346	-6.60829	10.2752	8.516	14.835	11.063	90.000	90.957	90.000	170	5	53
8.5159	14.9830	-6.60819	10.3779	8.516	14.983	11.063	90.000	90.957	90.000	266	1	54
8.5159	15.1313	-6.60803	10.4807	8.516	15.131	11.063	90.000	90.957	90.000	423	6	55
8.3530	14.8963	-6.60846	10.1205	8.353	14.896	11.063	90.000	90.938	90.000			predicted
8.3490	14.8346	-6.60845	10.0737	8.349	14.835	11.063	90.000	90.938	90.000	9	-1	cg3

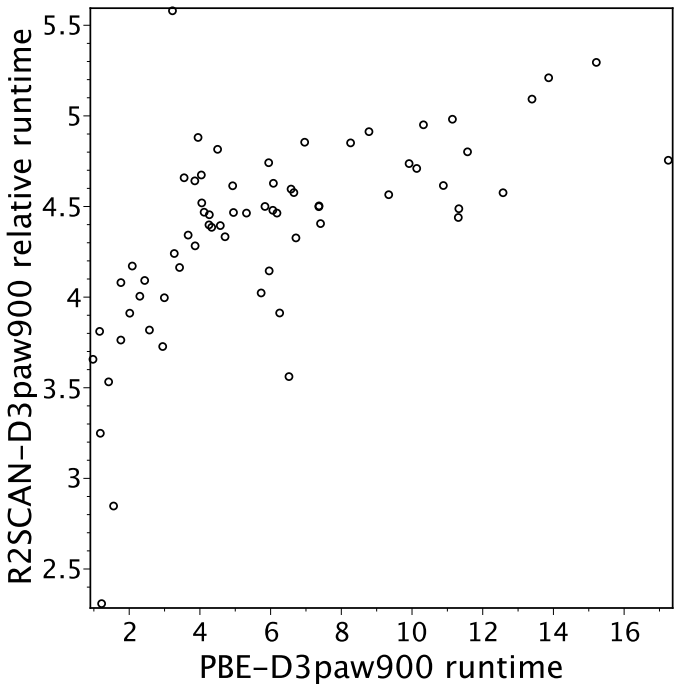

Figure S9: Runtime: R2SCAN vs PBE [URL].

Table S15: Comparison medium accuracy wrt high accuracy PBE-D3paw900 [URL].

system	na1	no	ns	SG	V1	dV1	dSh	dTv	da	db	dc	dalp	dbet	dgam	dr	phi	dev
str	#	#	#	str	Ao3	%	%	%	%	%	%	deg	deg	deg	mAo	deg	mAo
median						0.4	0.6	0.6	0.1	0.3	0.2	0.0	-0.0	0.0	0	0.5	3
mean						0.4	0.7	0.8	0.1	0.2	0.1	-0.0	-0.1	-0.0	3	0.6	5
standard dev						0.4	0.6	0.6	0.7	0.8	0.6	0.2	0.4	0.0	7	0.5	5
lower decile						-0.2	0.2	0.3	-0.9	-0.7	-0.7	0.0	-0.6	0.0	0	0.2	1
upper decile						0.9	1.3	1.4	0.7	1.2	0.7	0.0	0.5	0.0	12	1.3	10
min						-0.8	0.0	0.1	-1.5	-2.4	-2.0	-1.0	-0.9	-0.3	0	0.1	0
max						1.4	3.2	3.2	3.0	2.9	1.2	0.7	0.9	0.2	32	2.6	29
anthracene	24	1	2	P21/c	9.38	1.2	1.2	1.1	-0.2	1.8	-0.7	0.0	-0.7	0.0	0	0.7	1
anthraquinone	24	1	2	P21/c	9.67	-0.1	0.5	0.5	0.6	-0.9	-0.0	0.0	-0.3	0.0	0	0.4	2
benzene	12	1	2	Pbca	9.54	1.4	0.2	0.5	0.2	0.6	0.6	0.0	0.0	0.0	0	0.5	0
benzeneF6	12	2	1	P21/n	13.26	-0.7	0.4	0.5	0.3	-0.8	-0.2	0.0	-0.0	0.0	0	0.6	1
benzeneO2	12	1	2	P21/c	10.70	0.4	0.9	0.9	-0.3	1.0	-0.1	0.0	0.9	0.0	0	1.8	1
benzodithiopheneO2	18	1	2	P21/n	11.82	0.6	0.5	0.6	-0.5	0.6	0.5	0.0	-0.2	0.0	0	0.4	3
benzotrithiophene	21	1	1	P21/n	12.45	0.1	0.5	0.5	-0.3	-0.2	0.7	0.0	0.2	0.0	9	0.6	6
benzotrithiopheneA	21	2	1	P21	12.11	0.3	0.6	0.6	0.2	0.4	-0.4	0.0	-0.4	0.0	32	0.4	4
bithiophene	16	1	2	P21/c	11.72	0.4	1.6	1.5	0.9	0.9	-1.7	0.0	-0.7	0.0	0	2.2	1
BODIPY	21	1	1	C2/c	9.97	-0.2	0.9	0.9	-0.8	-0.4	0.9	0.0	-0.4	0.0	23	1.1	18
BTBT	24	1	2	P21/c	10.91	0.6	0.2	0.4	0.3	0.0	0.3	0.0	0.1	0.0	0	0.2	1
C60	60	1	6	Pa-3	11.70	-0.3	0.0	0.1	-0.1	-0.1	-0.1	0.0	0.0	0.0	0	0.2	0
carbazole	22	1	2	Pnma	9.21	0.3	0.7	0.8	-0.9	0.5	0.6	0.0	0.0	0.0	6	0.7	1
carbazoleNO2b	24	1	1	P21/n	9.96	-0.2	0.9	1.0	-0.4	1.0	-0.5	0.0	0.8	0.0	2	0.8	7
chrysene	30	1	2	C12/n1	9.38	0.6	0.9	0.9	0.1	1.7	-0.9	0.0	0.7	0.0	0	0.5	5
coronene	36	1	2	P21/n	9.57	0.0	0.6	0.6	0.4	-0.7	0.4	0.0	0.2	0.0	0	0.2	1
DATT	48	1	1	P21	9.98	0.3	0.6	0.6	0.6	-0.8	0.4	0.0	-0.2	0.0	12	0.4	8
DBTTF	26	1	2	P21/c	11.69	0.3	0.3	0.4	0.3	-0.4	0.3	0.0	-0.1	0.0	0	0.5	1
dibenzoindigo	42	1	2	P21/n	9.59	0.1	3.2	3.2	-1.2	1.9	-0.5	0.0	0.5	0.0	0	1.5	10
DNBDT	42	1	2	P21/n	9.94	0.4	0.3	0.4	0.4	-0.2	0.3	0.0	-0.0	0.0	0	0.2	4
DNTT	36	1	1	P21	10.39	0.6	0.4	0.5	0.3	-0.2	0.5	0.0	0.0	0.0	5	0.3	5
hexacene	42	2	2	P-1	9.05	-0.3	1.2	1.2	0.2	-1.1	0.3	-1.0	-0.9	-0.1	0	1.2	3
HMTTF	28	1	1	P21/c	10.18	0.2	0.2	0.2	0.0	-0.0	0.3	0.0	-0.1	0.0	12	0.2	7
ICZb	32	1	2	P21/c	9.16	0.4	0.8	0.8	0.1	0.9	-0.7	0.0	-0.8	0.0	0	0.7	4
ICZbCl2c	32	1	2	P21/c	10.34	0.0	0.8	0.8	0.1	1.1	-1.2	0.0	-0.3	0.0	0	1.5	7
IF12b	34	1	2	P21/n	9.17	0.6	1.1	1.0	-0.1	1.3	-0.6	0.0	0.8	0.0	0	0.6	5
IF21a	34	1	1	P21/c	9.58	0.7	0.7	0.8	-0.9	1.2	0.3	0.0	0.5	0.0	7	0.7	3
indigo	30	1	2	P21/n	9.59	0.4	0.8	0.8	0.1	0.8	-0.8	0.0	-0.4	0.0	0	0.5	3
indigoCl2	30	1	2	P21/c	11.01	0.4	0.6	0.5	-0.3	1.1	-0.2	0.0	0.2	0.0	0	0.3	3
naphthalene	18	1	2	P21/c	9.41	1.4	0.2	0.5	0.2	0.7	0.4	0.0	-0.1	0.0	0	0.3	0
NDFPh	44	1	2	P21/c	9.86	0.4	0.4	0.5	0.4	-0.5	0.4	0.0	-0.1	0.0	0	0.3	7
NDI	26	2	2	P-1	10.07	0.1	0.9	0.9	1.3	-0.4	-0.7	-0.1	-0.1	-0.3	0	0.8	7
NDT	24	2	2	P21/c	10.92	0.6	3.0	3.2	3.0	-2.4	-0.1	0.0	-0.6	0.0	0	2.6	4
oligothiophene4	30	1	2	P21/a	11.73	0.7	1.3	1.4	-1.3	0.6	1.2	0.0	-0.6	0.0	0	1.0	4
oligothiophene6	44	1	2	P21/a	11.70	0.1	1.1	1.1	-1.3	0.6	0.8	0.0	-0.1	0.0	0	1.3	13
OPV3CN	42	1	2	Pbca	10.12	0.2	0.4	0.5	0.1	-0.3	0.3	0.0	0.0	0.0	0	0.7	29
PBBTZ	30	1	1	P21/n	10.57	0.2	0.2	0.3	-0.1	0.2	0.1	0.0	0.1	0.0	2	0.1	2
PDI	40	1	2	P21/n	9.64	0.3	0.5	0.5	-0.0	0.5	-0.2	0.0	-0.2	0.0	0	0.2	3
pentacene	36	2	2	P-1	9.17	0.3	0.8	0.8	-0.7	1.1	0.1	-0.5	-0.4	0.2	0	0.7	3
pentaceneN2Cl4	34	1	2	P21/n	11.88	0.8	0.8	1.0	-0.4	1.3	-0.0	0.0	-0.1	0.0	0	0.2	5
pentaceneN4O2	32	1	2	P21/n	9.92	-0.0	0.3	0.3	-0.4	0.4	-0.1	0.0	0.1	0.0	0	0.2	3
perylene	32	1	2	P21/c	9.16	1.1	2.1	2.0	0.2	2.9	-2.0	0.0	-0.6	0.0	0	1.3	3
phenazine	22	1	2	P21/n	9.75	0.9	0.4	0.5	0.7	0.3	-0.1	0.0	0.3	0.0	0	1.6	2
PTCDA	38	1	2	P21/c	10.10	-0.1	0.5	0.5	-0.3	0.4	-0.3	0.0	-0.4	0.0	0	0.7	3
pyrene	26	1	1	P21/a	9.60	0.3	1.4	1.4	-1.5	1.2	0.5	0.0	-0.6	0.0	10	1.2	2
quinacridone	36	1	2	P21/c	9.47	0.9	1.5	1.7	1.6	-0.7	0.3	0.0	0.8	0.0	0	0.9	6
spirobidibenzosilole	41	1	2	P41212	10.43	0.6	0.2	0.4	0.1	0.1	0.3	0.0	0.0	0.0	3	0.3	12
spirobifluorene	41	1	1	P21/c	10.11	0.3	0.2	0.2	-0.0	0.4	-0.1	0.0	0.0	0.0	17	0.2	7
stilbene	26	2	2	P21/a	9.37	0.8	1.1	1.1	1.3	0.2	-0.4	0.0	0.4	0.0	0	0.5	3
TCNQ	20	1	2	C2/c	12.42	0.6	0.6	0.5	0.4	0.6	-0.3	0.0	0.4	0.0	0	0.9	3
TCNQ-F2	20	1	4	C2/m	12.84	0.1	0.4	0.4	0.1	-0.3	0.5	0.0	0.3	0.0	0	0.2	3
TCNQ-F4	20	1	2	Pbca	13.90	-0.5	1.1	1.1	-0.9	-0.8	1.1	0.0	0.0	0.0	0	0.7	6
tetracene	30	2	2	P-1	9.30	0.6	1.1	1.1	1.2	-1.0	0.4	0.7	-0.4	-0.0	0	0.7	1
thiazolothiazolePh	30	1	2	P21/c	10.70	1.0	0.8	1.3	-0.7	0.7	0.8	0.0	-0.4	0.0	0	1.1	5
TPP	34	1	1	P21/c	10.07	0.4	0.4	0.4	-0.0	-0.3	0.6	0.0	-0.1	0.0	16	0.4	20
triazine	9	1	2	C2/c	10.20	-0.8	0.2	0.4	-0.3	-0.2	-0.6	0.0	-0.2	0.0	0	0.1	1
triphenylbenzene	42	1	1	Pna21	9.55	0.7	0.3	0.5	-0.2	0.5	0.4	0.0	0.0	0.0	5	0.1	8
triphenylene	30	1	1	P212121	9.25	0.0	0.4	0.4	-0.2	-0.2	0.4	0.0	0.0	0.0	11	0.4	3
triphenyltriazine	39	1	1	P21/c	9.43	0.4	0.4	0.6	0.4	-0.3	0.3	0.0	-0.0	0.0	9	0.1	7
triptycene	34	1	1	P212121	9.77	1.0	0.1	0.3	0.3	0.5	0.2	0.0	0.0	0.0	6	0.1	3
TTAa	36	1	2	P21/n	11.27	0.5	0.2	0.3	-0.1	0.4	0.2	0.0	0.2	0.0	0	0.2	2
TTAb	36	1	2	P21/n	11.25	0.5	0.5	0.4	0.0	0.7	-0.3	0.0	-0.3	0.0	0	0.2	2
TTF	14	1	2	P21/c	13.51	0.4	0.9	1.0	0.1	-0.5	0.5	0.0	-0.9	0.0	0	1.2	3
TTPa	34	1	2	P21/n	11.67	0.0	0.3	0.3	-0.1	0.2	-0.1	0.0	0.2	0.0	0	0.2	3
TTPb	34	2	2	P21/a	11.83	-0.0	0.4	0.3	0.3	-0.4	0.1	0.0	0.1	0.0	0	0.4	3
TTPc	34	1	1	P21	11.92	0.5	0.5	0.7	0.2	-0.5	0.8	0.0	-0.1	0.0	29	0.4	13
TTTT	18	1	2	P21/n	12.70	0.3	0.6	0.7	0.6	-0.4	0.3	0.0	0.4	0.0	0	0.2	1

Table S16: Smaller cutoff with unconstrained relaxation for PBE-D3 [URL].

Unconstrained relaxation of unit cell (cg3) at 600eV compared to 900eV and volume scan at 600eV:

system	600cg3	900cg3	600vs	
anthraquinone	9.443	9.669	9.733	
benzene	9.270	9.544	9.575	
benzeneF6	12.575	13.261	13.395	* difference is 6%
naphthalene	9.163	9.413	9.449	
pentacene	8.968	9.169	9.242	
TCNQ	12.184	12.424	12.507	
triazine	9.966	10.202	10.227	
triphenylbenzene	9.314	9.549	9.597	

Table S17: Gradients at optimized geometry: PBE-D3paw900 [URL].

cg3, N=67, gradient in meV/Ao, 2023-04-10

	optimization			SP		finerSP	
	nopt	|G|	maxG	|G|	maxG	|G|	maxG
anthracene	1	1	1	0	1	0	1
anthraquinone	75	1	1	1	1	1	1
benzene	5	1	1	1	1	1	1
benzeneF6	9	1	1	1	1	1	1
benzeneO2	7	1	1	1	1	1	1
benzodithiopheneO2	96	1	1	1	1	1	1
benzotrithiophene	93	0	1	1	1	1	1
benzotrithiopheneA	1	0	1	1	1	1	1
bithiophene	1	1	1	1	1	1	1
BODIPY	8	0	1	1	1	1	1
BTBT	41	1	1	1	1	1	1
C60	5	1	1	1	1	1	1
carbazole	1	0	1	0	1	0	1
carbazoleNO2b	1	0	1	0	1	0	1
chrysene	35	1	1	1	1	1	1
coronene	1	1	1	1	1	1	1
DATT	1	1	1	1	1	1	1
DBTTF	5	1	1	1	1	1	1
dibenzoindigo	9	0	1	0	1	0	1
DNBDT	1	0	1	0	1	0	1
DNTT	4	1	1	1	1	1	1
hexacene	1	0	1	1	1	1	1
HMTTF	39	1	1	1	1	1	1
ICZb	3	1	1	1	1	1	1
ICZbCl2c	74	0	1	1	1	1	1
IF12b	1	1	1	1	1	1	1
IF21a	1	1	1	1	1	1	1
indigo	39	1	1	1	1	1	1
indigoCl2	1	1	1	1	1	1	1
naphthalene	1	1	1	1	1	1	1
NDFPh	1	1	1	1	1	1	1
NDI	5	0	1	0	1	0	1
NDT	1	1	1	1	1	1	1
oligothiophene4	6	1	1	1	1	1	1
oligothiophene6	27	1	1	1	1	1	1
OPV3CN	5	1	1	1	1	1	1
PBBTZ	81	0	1	0	1	1	1
PDI	1	1	1	1	1	1	1
pentacene	6	0	1	0	1	0	1
pentaceneN2Cl4	3	1	1	1	1	1	1
pentaceneN4O2	1	1	1	1	1	1	1
perylene	1	1	1	1	1	1	1
phenazine	47	1	1	1	1	1	1
PTCDA	36	0	1	0	1	0	1
pyrene	8	1	1	1	1	1	1
quinacridone	54	1	1	1	1	1	1
spirobidibenzosilole	47	0	1	1	1	1	1
spirobifluorene	7	1	1	1	1	1	1
stilbene	1	1	1	1	1	1	1
TCNQ	1	0	1	1	1	1	1
TCNQ-F2	6	1	1	1	1	1	1
TCNQ-F4	8	0	1	1	1	1	1
tetracene	83	0	1	1	1	1	1
thiazolothiazolePh	9	0	1	0	1	0	1
TPP	4	1	1	1	1	1	1
triazine	34	1	1	1	1	1	1
triphenylbenzene	12	1	1	1	1	1	1
triphenylene	3	0	1	0	1	0	1
triphenyltriazine	1	1	1	1	1	1	1
triptycene	1	0	1	0	1	0	1
TTAa	7	1	1	1	1	1	1
TTAb	1	1	1	1	1	1	1
TTF	69	1	1	1	1	1	1
TTPa	3	0	1	1	1	1	1
TTPb	7	1	1	1	1	1	1
TTPc	58	1	1	1	1	1	1
TTTT	9	1	1	1	1	1	1

Table S18: Comparison of different k-grids (PBE-D3paw900) [URL].

Comparison of different k-grids
method=PBE-D3paw900
exp=relaxed from experimental geometry
100812=10x8x12 k-grid

	V	a	b	c	alpha	beta	gamma
--- anthraquinone (P21/c) ---							
482	9.669	7.834	3.862	15.713	90	102.53	90
241	9.675	7.837	3.863	15.715	90	102.55	90
222	9.902	7.677	4.167	15.392	90	105.14	90
221	9.906	7.677	4.168	15.394	90	105.13	90
111	9.270	4.776	6.102	17.518	90	119.36	90
--- benzene (Pbca) ---							
100812	9.544	7.322	9.328	6.708	90	90	90
646	9.544	7.322	9.328	6.708	90	90	90
323	9.544	7.322	9.328	6.708	90	90	90
222	9.543	7.321	9.326	6.708	90	90	90
222(exp)	9.551	7.320	9.326	6.715	90	90	90
111	9.944	10.976	8.995	4.835	90	90	90
--- benzeneF6 (P21/n) ---							
642	13.261	5.976	9.368	17.096	90	94.01	90
222	13.269	5.980	9.405	17.030	90	94.11	90
221	13.272	5.976	9.375	17.100	90	94.06	90
111	12.046	4.274	9.831	21.744	90	108.30	90
--- BTBT (P21/c) ---							
365	10.915	11.790	5.887	7.844	90	105.78	90
222	10.900	11.788	5.866	7.862	90	105.76	90
111	10.030	12.006	4.583	9.179	90	107.59	90
--- naphthalene (P21/c) ---							
454	9.413	7.812	5.902	8.064	90	114.29	90
222	9.417	7.801	5.919	8.048	90	114.17	90
111	8.904	9.941	4.583	8.683	90	125.88	90
--- NDI (P-1) ---							
444	10.068	7.527	8.225	9.066	89.77	71.61	79.89
222	10.082	7.526	8.233	9.067	89.79	71.71	79.84
111	9.911	8.022	8.388	8.211	89.90	74.20	76.34
--- pentacene (P-1) ---							
542	9.169	6.252	7.620	14.291	77.08	88.79	84.17
222	9.167	6.265	7.613	14.271	77.09	88.90	84.12
221	9.184	6.257	7.625	14.308	76.89	88.93	84.11
111	8.173	4.360	8.796	16.838	71.29	75.03	89.99
--- TCNQ (C2/c:P) ---							
662	12.424	8.848	6.876	16.483	90	97.59	90
222	12.440	8.886	7.008	16.120	90	97.54	90
111	8.418	7.682	4.723	18.807	90	99.28	90
--- TCNQ-F2 (C2/m:P) ---							
774	12.837	10.199	5.951	8.817	90	106.37	90
222	12.884	10.201	5.954	8.826	90	105.99	90
111	10.222	8.353	5.534	8.965	90	99.40	90

S6 Additional figures and tables for approximate DFT methods

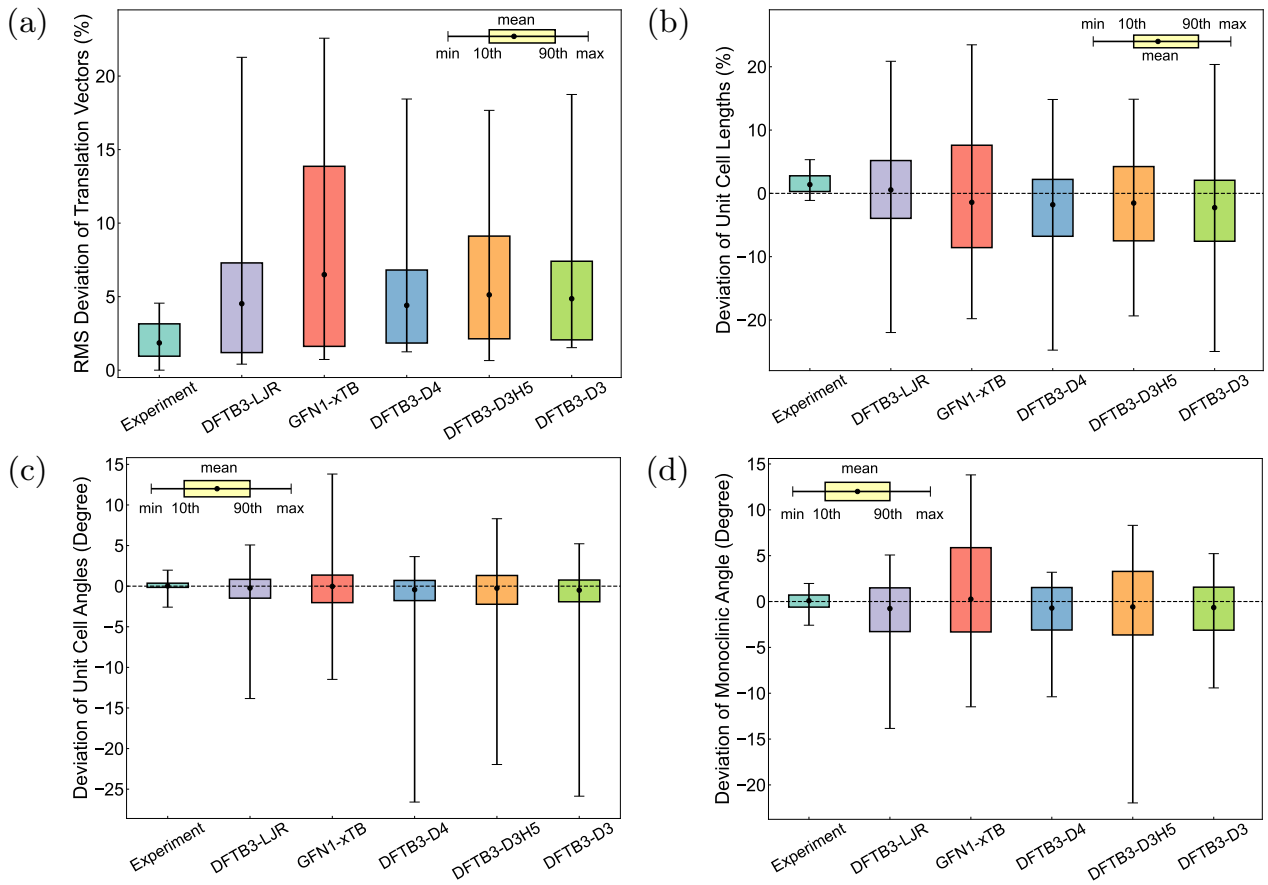

Figure S10: Benchmark of approximate DFT methods against DFT (r^{2}SCAN-D3) reference. (a) The RMS deviation of translation vectors, (b) deviation of unit cell lengths a, b and c, (c) deviation of unit cell angles α, β and γ, (d) deviation of monoclinic angle β.

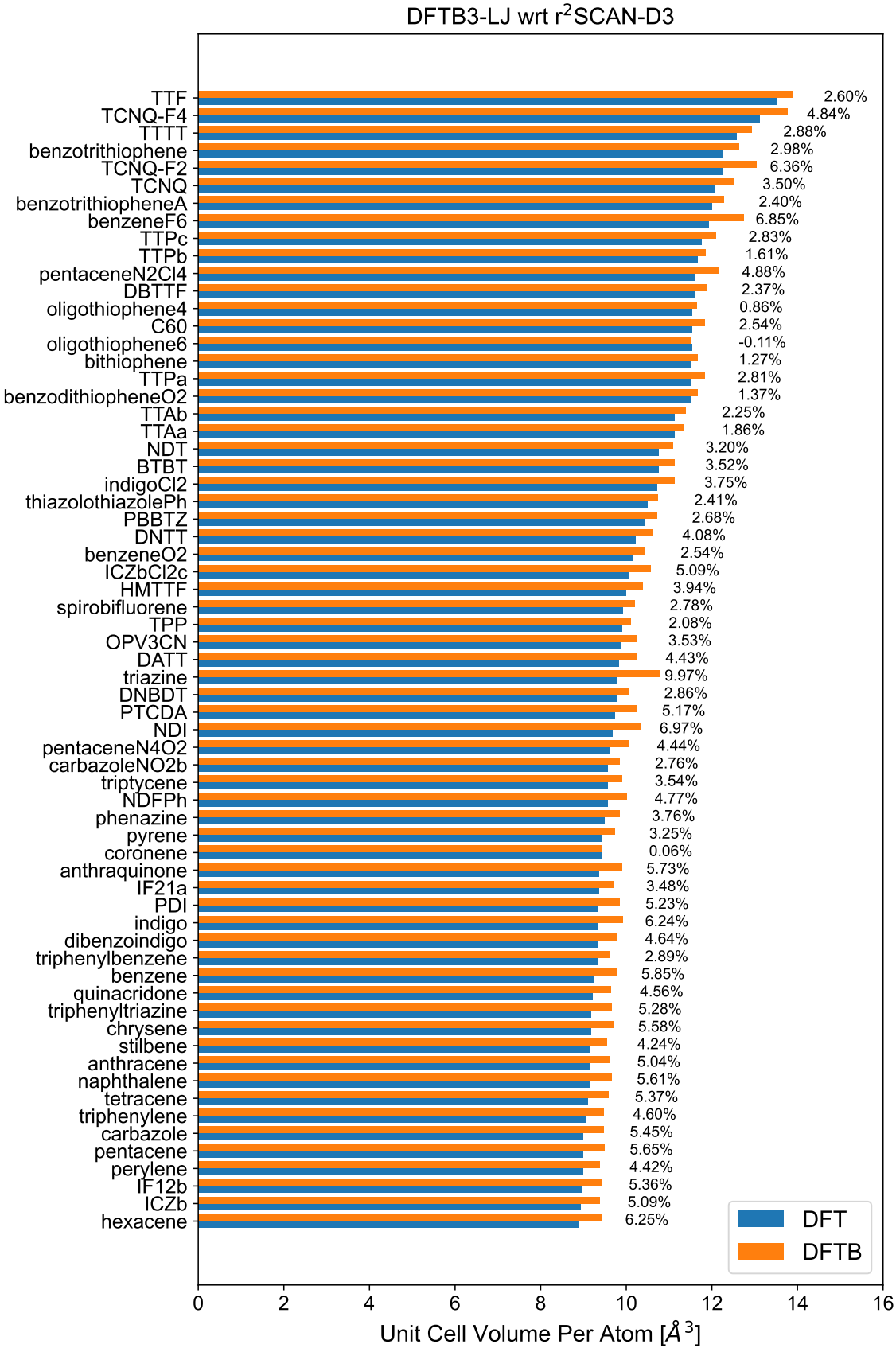

Figure S11: Comparison between DFTB3-LJ with original parameters and DFT reference on unit cell volume. The average error is 3.92%.

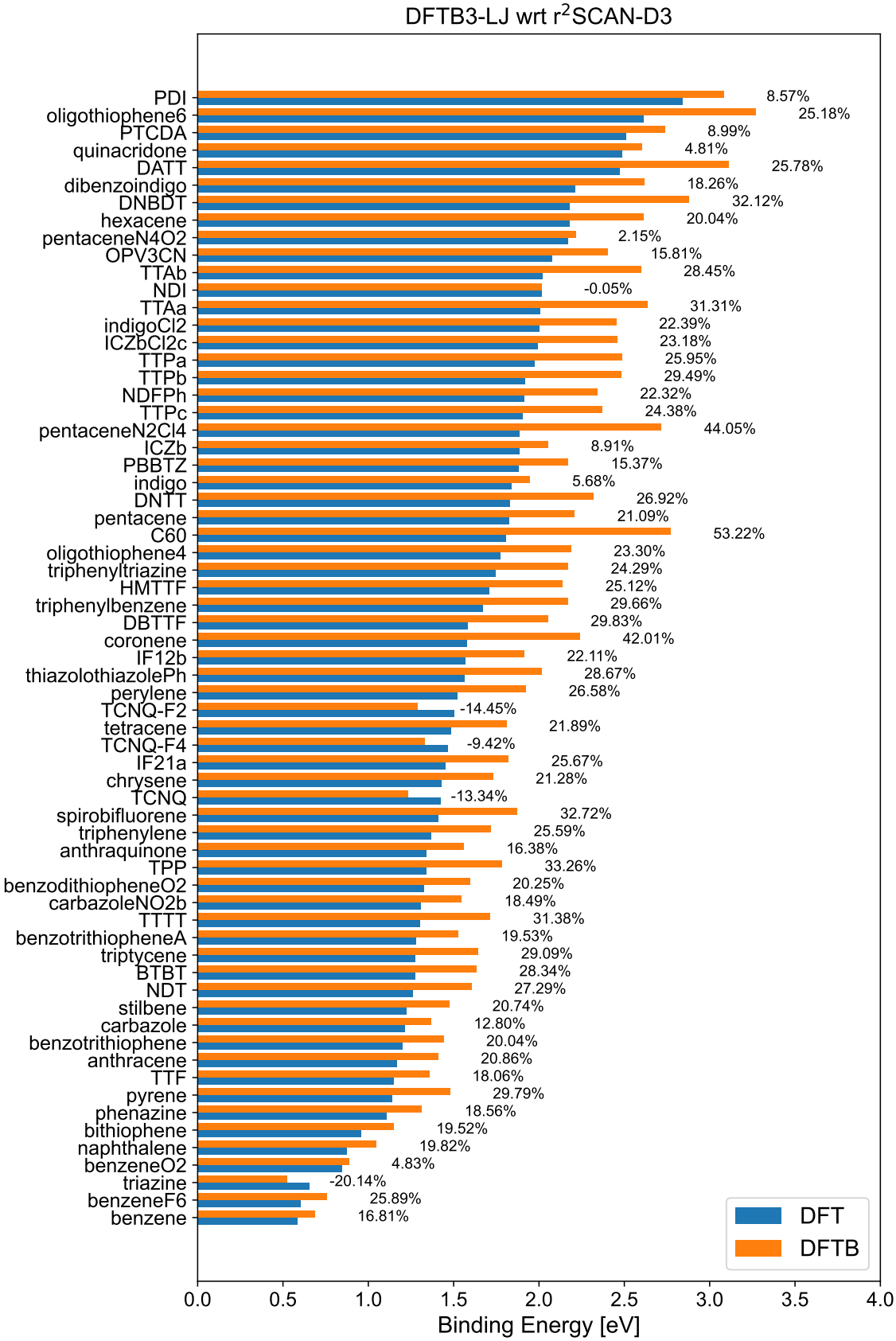

Figure S12: Comparison between DFTB3-LJ with original parameters and DFT reference on binding energy. The average error is 20.30%.

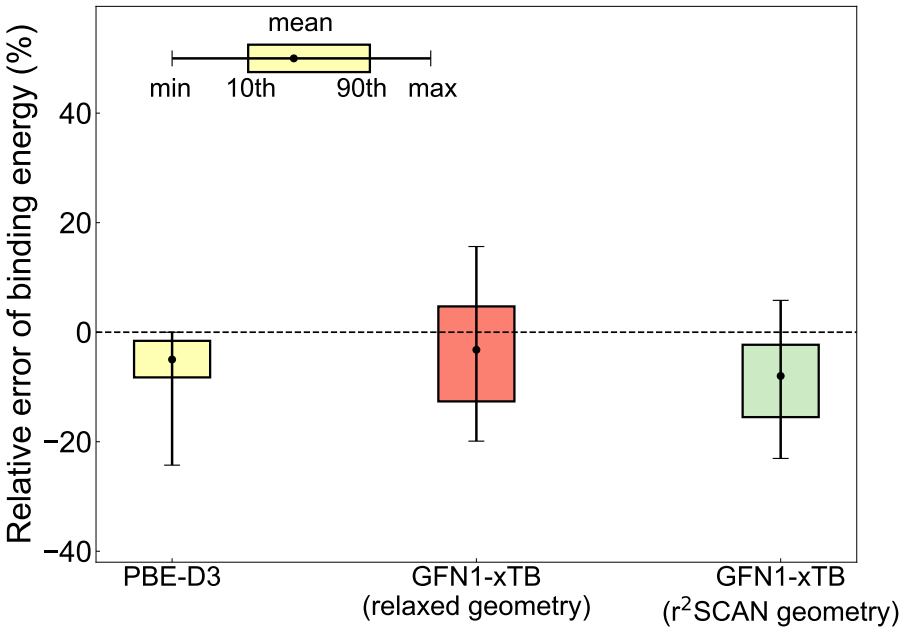

Figure S13: The comparison of binding energies calculated by GFN1-xTB using relaxed geometries and r^{2}SCAN geometries.

Table S19: The groupings of crystals based on chemical features.

Group name and description	Chemical feature	System
C – hydrocarbons	C	anthracene
	C	benzene
	C	C60
	C	chrysene
	C	coronene
	C	hexacene
	C	IF12b
	C	IF21a
	C	naphthalene
	C	pentacene
	C	perylene
	C	pyrene
	C	stilbene
	C	tetracene
	C	triphenylbenzene
	C	triphenylene
	CCsp3	spirobifluorene
	CCsp3	triptycene
CS – molecules with sulfur in aromatic rings	CS	benzotrithiophene
	CS	benzotrithiopheneA
	CS	bithiophene
	CS	BTBT
	CS	DATT
	CS	DBTTF
	CS	DNBDT
	CS	DNTT
	CS	HMTTF
	CS	NDT
	CS	oligothiophene4
	CS	oligothiophene6
	CS	TTAa
	CS	TTAb
	CS	TTF
	CS	TTTT
CN – molecules with nitrogen in aromatic rings	CN	carbazole
	CN	ICZb
	CN	phenazine
	CN	triazine
	CN	triphenyltriazine
CO – molecules with π-conjugated oxygen atoms	C(O)	anthraquinone
	CO	NDFPh
	CO(O)	PTCDA
	C(O)	benzeneO2
CNH(O) – this group contains a wide range of structures incorporating carbon, nitrogen, and hydrogen in their backbone structure, and in some cases carbonyl or nitro substituents	CN(O)	pentaceneN4O2
	CNH(O)	dibenzoindigo
	CNH(O)	indigo
	CNH(O)	NDI
	CNH(O)	PDI
	CNH(O)	quinacridone
	CNH(NO2)	carbazoleNO2b
CNS – structures with carbon, nitrogen, and sulphur	CNS	thiazolothiazolePh
	CNS	TTPa
	CNS	TTPb
	CNS	TTPc
CNBF – structures with C, N, B, and F	CNBF	BODIPY
C(CN) – structures with cyano groups	C(CN)	OPV3CN
	C(CN)	TCNQ
F – molecules with fluorine atoms	C(F)	benzeneF6
	C(CN)F	TCNQ-F2
	C(CN)F	TCNQ-F4
Cl – molecules with chlorine atoms	CNH(O)Cl	indigoCl2
	CNCl	ICZbCl2c
	CNCl	pentaceneN2Cl4
Other molecules	CS(O)	benzodithiopheneO2
	CSNNH	PBBTZ
	CSi	spirobidibenzosilole
	CP	TPP

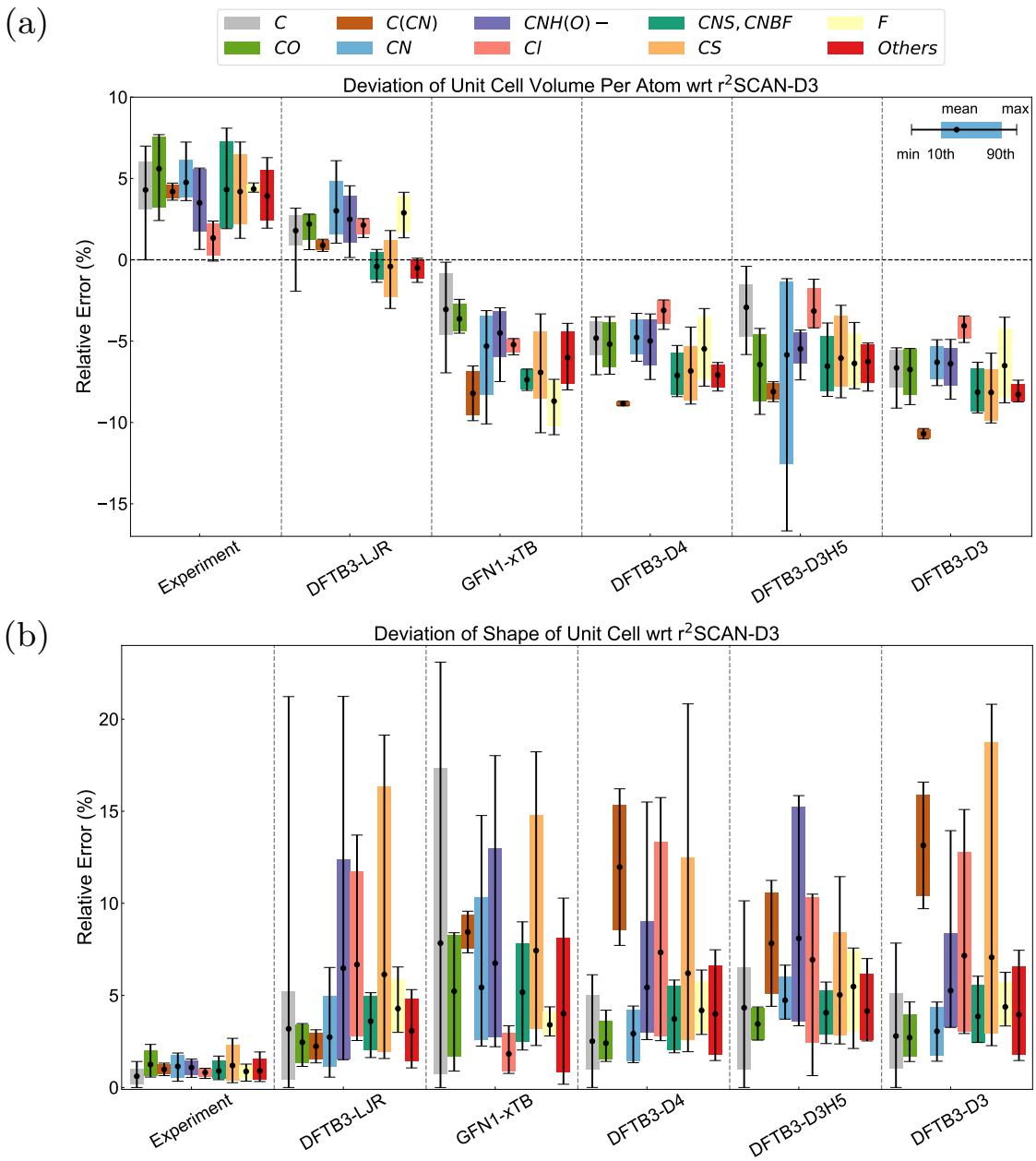

Figure S14: Performance of the approximate DFT methods on different groups of crystals. The deviations of (a) unit cell volume per atom and (b) shape of unit cell.

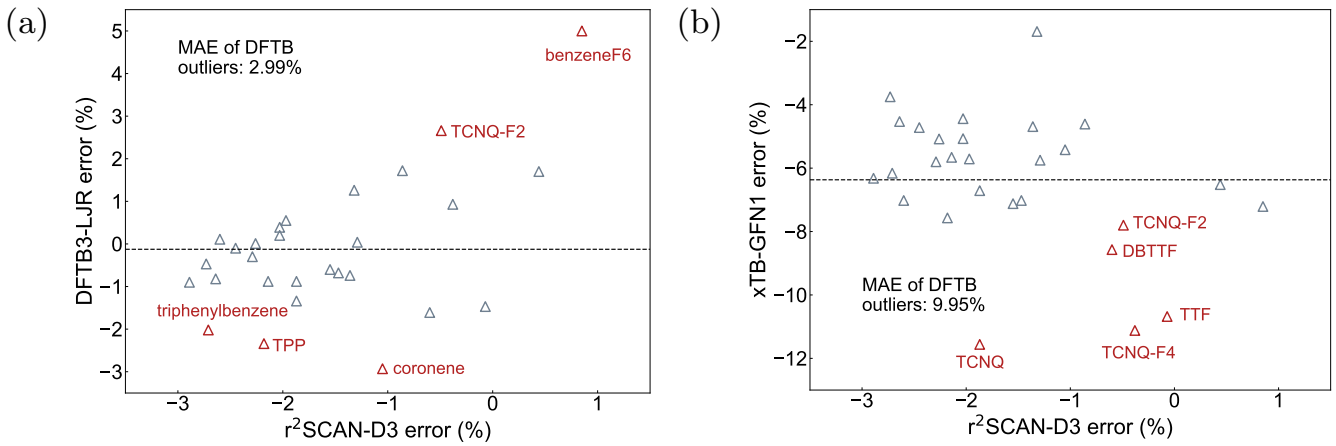

Figure S15: (a) The comparison between the error of r^{2}SCAN-D3 and DFTB3-LJR in terms of unit cell volume per atom, using experimental results with extrapolated volumes (zero temperature) as the reference. (b) The comparison between the error of r^{2}SCAN-D3 and xTB-GFN1 in terms of unit cell volume per atom, using experimental results with extrapolated volumes (zero temperature) as the reference. In the plots, the red triangles represent 5 systems exhibiting the highest absolute errors, which are identified as the outliers for the two approximate DFT methods. The gray triangles indicate the remaining systems. The black dashed line displays the mean error of the DFTB3-LJR/xTB-GFN1 method. For comparison, the mean absolute error (MAE) of the 5 outliers for the DFTB3-LJR and the xTB-GFN1 method is 2.99% and 9.95%, respectively.